Author Manuscript

Author Manuscript

Author Manuscript

Author Manuscript

HHS Public Access

Author manuscript

Cell Rep. Author manuscript; available in PMC 2022 November 06.

Published in final edited form as:

Cell Rep. 2022 October 18; 41(3): 111489. doi:10.1016/j.celrep.2022.111489.

IL-17-induced dimerization of IL-17RA drives the formation of the IL-17 signalosome to potentiate signaling

Arnaud Goepfert[1,4], **Carmen Barske**[1], **Sylvie Lehmann**[1], **Emmanuelle Wirth**[1], **Joschka Willemsen**[1], **Johann E. Gudjonsson**[2], **Nicole L. Ward**[3], **Mrinal K. Sarkar**[2], **René Hemmig**[1], **Frank Kolbinger**[1], **Jean-Michel Rondeau**[1,5,*]

[1]Novartis Institutes for BioMedical Research, Novartis Pharma AG, 4002 Basel, Switzerland

[2]Department of Dermatology, University of Michigan, Ann Arbor, MI, USA

[3]Department of Dermatology, Vanderbilt University Medical Center, Nashville, TN, USA

[4]Present address: Bright Peak Therapeutics, 4057 Basel, Switzerland

[5]Lead contact

SUMMARY

Signaling through innate immune receptors such as the Toll-like receptor (TLR)/interleukin-1 receptor (IL-1R) superfamily proceeds via the assembly of large membrane-proximal complexes or "signalosomes." Although structurally distinct, the IL-17 receptor family triggers cellular responses that are typical of innate immune receptors. The IL-17RA receptor subunit is shared by several members of the IL-17 family. Using a combination of crystallographic, biophysical, and mutational studies, we show that IL-17A, IL-17F, and IL-17A/F induce IL-17RA dimerization. X-ray analysis of the heteromeric IL-17A complex with the extracellular domains of the IL-17RA and IL-17RC receptors reveals that cytokine-induced IL-17RA dimerization leads to the formation of a 2:2:2 hexameric signaling assembly. Furthermore, we demonstrate that the formation of the IL-17 signalosome potentiates IL-17-induced IL-36γ and CXCL1 mRNA expression in human keratinocytes, compared with a dimerization-defective IL-17RA variant.

In brief

This is an open access article under the CC BY-NC-ND license (http://creativecommons.org/licenses/by-nc-nd/4.0/).

*Correspondence: jeanmichel.rondeau@novartis.com.

AUTHOR CONTRIBUTIONS

A.G. and J.-M.R. designed crystallographic experiments and analyzed data; A.G. and S.L. performed protein purification and crystallization experiments; A.G. and E.W. performed biophysical experiments and analyzed data; R.H. produced refolded IL-17A(31–155) and helped with SEC-MALS analyses; J.E.G., M.K.S., and N.L.W. generated the IL-17RA KO N/TERT cell line; J.W. generated WT and mutant IL-17RA N/TERT cells; C.B. performed and analyzed cellular experiments; F.K. designed cellular experiments and analyzed cellular data; all authors contributed to the writing of the manuscript.

DECLARATION OF INTERESTS

A.G. is a former employee of Novartis Pharma AG, Switzerland. C.B., S.L., E.W., J.W., R.H., F.K. and J.-M.R. are employees and shareholders of Novartis Pharma AG, Switzerland.

INCLUSION AND DIVERSITY

We support inclusive, diverse, and equitable conduct of research.

SUPPLEMENTAL INFORMATION

Supplemental information can be found online at https://doi.org/10.1016/j.celrep.2022.111489.

Author Manuscript
Author Manuscript
Author Manuscript
Author Manuscript

IL-17RA is the shared co-receptor for several IL-17 family members. Goepfert et al. show that IL-17 induces IL-17RA dimerization, which then drives the formation of a 2:2:2 hexameric signaling assembly with IL-17RC. Furthermore, IL-17RA dimerization potentiates IL-17 signaling in immortalized primary human keratinocytes, compared with cells expressing a dimerization-defective IL-17RA variant.

Graphical Abstract

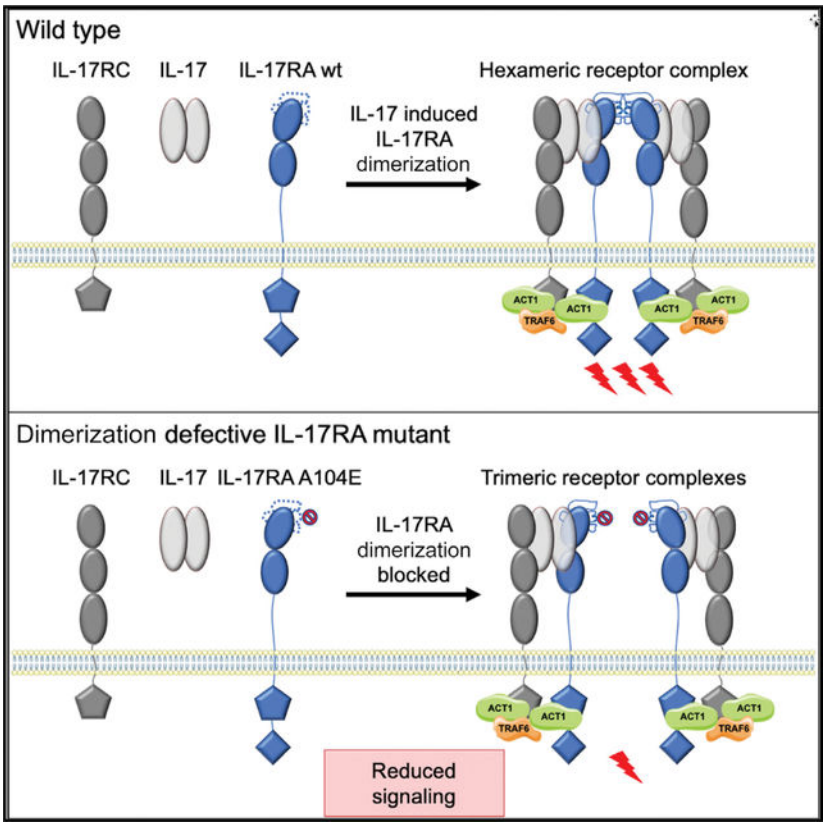

INTRODUCTION

The IL-17 family of pro-inflammatory cytokines is an important player in both adaptive and innate immunity (Gaffen et al., 2014; Veldhoen, 2017). The best characterized members to date are the homodimeric IL-17A, IL-17E (also known as IL-25), and IL-17F cytokines, which are produced by many cell populations of the innate immune system, notably in the skin, lung, and mucosal barriers, and contribute to the early inflammatory and innate immune responses against stress, injury, or extracellular pathogens (Cua and Tato, 2010). While IL-17E is also produced by effector T helper type 2 (Th2) cells and augments Th2-type immune responses (Deng et al., 2021), IL-17A and IL-17F are the signature cytokines of Th17 cells that regulate the adaptive immune response to extracellular bacteria and fungi (Korn et al., 2009). Besides their normal physiological role, Th17 cells have been implicated in a broad range of chronic inflammatory diseases, autoimmune disorders, and cancers (McGeachy et al., 2019; Majumder and McGeachy, 2021; Chung et al., 2021). Recently,

Author Manuscript Author Manuscript Author Manuscript Author Manuscript

several components of the Th17 pathway have been successfully targeted for therapeutic intervention, notably IL-17A and the IL-17RA receptor (Patel and Kuchroo, 2015; Beringer et al., 2016).

IL-17RA is shared by several IL-17 family members, including IL-17A, IL-17C, IL-17E, IL-17F, and the IL-17A/F heterodimer. Signaling through IL-17RA requires the formation of a heteromeric receptor complex with either IL-17RB (IL-17E), IL-17RC (IL-17A, IL-17F, IL-17A/F), IL-17RD (IL-17A), or IL-17RE (IL-17C). The exact composition of these signaling complexes has not been firmly established to date (Krstić et al., 2015). IL-17RA, IL-17RB, and IL-17RD have short extracellular domains (ECD), whereas IL-17RC and IL-17RE are so-called “tall” receptors (Goepfert et al., 2020; Skiniotis et al., 2005). The association of short receptors with tall receptors has been documented for other cytokines such as IL-6 and IL-23, both of which, however, use a tall receptor (gp130 and IL-12Rβ1, respectively) as shared receptor (Wang et al., 2009; Glassman et al., 2021).

All members of the IL-17 receptor (IL-17R) family are single-pass type I membrane proteins typified by an intracellular signaling motif, the SEFIR domain (Novatchkova et al., 2003). This domain shows some similarities to the Toll/IL-1R (TIR) domain found in Toll-like receptors (TLR) and IL-1 receptors (IL-1R) as well as in cytoplasmic adaptor proteins recruited by these receptors. Upon TLR/IL-1R receptor activation, the TIR domain mediates TIR-TIR homotypic interactions, resulting in the recruitment of TIR and death-domain (DD)-containing bifunctional adaptor proteins, which, in turn, drive the formation of large membrane-proximal complexes or “signalosomes” through subsequent DD-DD interactions (Ferrao et al., 2012). While IL-17 signaling does not involve any DD-containing proteins, the SEFIR domain plays a similar role as the TIR domain in mediating the initial, membrane-proximal recruitment of the multifunctional adaptor protein, Act1, through SEFIR-SEFIR interactions (Chang et al., 2006; Qian et al., 2007). Act1 controls both the transcriptional as well as the post-transcriptional regulation of IL-17 responsive genes, by recruiting and activating different TRAF proteins (TRAF6, TRAF2), and also by directly interacting with RNAs (Li et al., 2019). According to a recent study, the IL-17A/IL-17RA/IL-17RC heterotrimeric receptor recruits approximately six ACT1 molecules, which provide high-avidity docking sites for TRAF6 homotrimers (Draberova et al., 2020). Non-degradative K63-linked polyubiquitination of TRAF6 by Act1 leads to the recruitment of downstream adaptor (ABIN1, TAX1BP1, TANK, NAP1), effector (TAK1, LUBAC, NEMO/IKKα/IKKβ), and regulatory proteins (IKKε, TBK1, A20, Cullin1, β-TrCP1/2) and ultimately to the activation of the NF-κB and MAP kinase pathways (Amatya et al., 2017; Li et al., 2019; Draberova et al., 2020).

While the TLR/IL-1R superfamily and the IL-17R family are both playing an important role in the regulation of the innate and inflammatory immune response, our understanding of the architecture and assembly mechanism of the IL-17 signaling complex remains comparatively very poor.

Here, we report the crystal structure of human IL-17RA in the unliganded state and show the presence of a conserved IL-17RA dimerization interface, which has remained unnoticed thus far in all previously published IL-17RA-IL-17 (A, F, A/F) binary complexes. We also

Author Manuscript Author Manuscript Author Manuscript Author Manuscript

disclose low-resolution crystallographic data on the extracellular portion of the IL-17A - IL-17RA - IL-17RC signalosome that firmly establish its composition and reveal that IL-17RA dimerization controls its architecture. Our structural inferences are corroborated by biochemical and biophysical studies of a dimerization-defective variant of IL-17RA. Using an IL-17RA knockout human keratinocyte cell line expressing either wild-type or the dimerization-defective IL-17RA mutant, we show that a functional consequence of IL-17-induced IL-17RA dimerization is a lower threshold for IL-17-induced mRNA expression of the downstream effector cytokines IL-36γ and CXCL1.

RESULTS

The X-ray analysis of IL-17RA in the free state reveals IL-17-induced domain motions

The unliganded, full-length extracellular domain (ECD) of human IL-17RA was expressed in GnTI-deficient HEK293S cells, purified, crystallized, and its three-dimensional structure determined at 1.90 Å resolution by molecular replacement (Tables S1 and S2 and Figure 1A). The IL-17RA ECD consists of two non-canonical fibronectin-III (FnIII) domains D1 and D2 connected by an 18-amino acid linker comprising a short α-helix (Ely et al., 2009). Previous X-ray analyses of IL-17RA binary complexes with IL-17F, IL-17A, or IL-17A/F have shown that both FnIII domains contact the cytokine through three main binding subsites, referred to as sites 1, 2, and 3 (Ely et al., 2009; Liu et al., 2013; Goepfert et al., 2017).

While the structures of IL-17RA in the free and cytokine-bound states are highly similar overall, unexpected structural changes within the amino-terminal FnIII domain (D1) as well as a change in the relative orientation of the two FnIII domains are revealed by the X-ray analysis of unliganded IL-17RA (Figure 1).

The linker region that connects the D1 and D2 domains appears to act as an elbow joint, allowing the fine adjustment of the relative orientation of the two FnIII domains in response to the various IL-17 cytokines. The corresponding elbow angle differs in the unliganded receptor and in the three known cytokine complexes (Figure 1B). In comparison to the ligand-free state, the binding of IL-17A, IL-17F, or IL-17A/F induces a rotation of the D2 domain of about 23°, 19°, and 30°, respectively (Figures 1B and 1D). The first 13 residues of the linker are rigidified by a disulfide bridge (Cys185–Cys196). The joint region begins at the following residue, Met197 (numbering scheme based on Uniprot: Q96F46). The D2 domain interacts with site 3, a surface binding site that comprises the C-terminal tail of one IL-17 (A, F, or A/F) subunit. The last five C-terminal residues, which are disordered in the free cytokines, adopt an extended conformation in the complex with IL-17RA and form sequence-independent, β-strand/ β-strand interactions with the D2 domain of the receptor (Ely et al., 2009; Liu et al., 2013; Goepfert et al., 2017). Together with the elbow motion of the receptor, the flexibility and the binding mode of the C-terminal tail of IL-17 (A, F, or A/F) ensure the formation of optimal interactions between the D2 domain of IL-17RA and its different ligands. In addition, the rotation of the D2 domain upon cytokine binding might play a role in the formation of the signaling-competent state.

Author Manuscript Author Manuscript Author Manuscript Author Manuscript

The D1 domain of IL-17RA undergoes cytokine-induced structural changes

The IL-17RA D1 domain interacts with IL-17 (A, F, or A/F) at two sites referred to as site 1 and site 2, both located at the cytokine dimer interface (Ely et al., 2009; Liu et al., 2013; Goepfert et al., 2017). While site 2 is largely preformed in the free cytokine, site 1 is a cryptic site that opens up upon receptor binding. Three receptor loops of the IL-17RA D1 domain, of which two play a role in cytokine binding at site 1 (A'A loop, residues 59–73, and FG loop, residues 166–174), are disordered in the free state (Figure 1). Notably, the ^{58}LDDSWI^{63} motif, which has been shown to provide critical binding interactions in site 1 (Ely et al., 2009; Liu et al., 2013; Goepfert et al., 2017), is disordered in the unliganded state. The side-chain of Leu58 is defined but pointing in a direction opposite to the cytokine-binding interface. In contrast, the CC′ loop (residues Leu117–Arg124) that inserts into site 2 is well-defined and in a conformation similar to that of the cytokine-bound state, albeit with a small (~1.5 Å) translational shift of its tip.

The X-ray structure of IL-17RA in the free state also reveals that the BC loop of the D1 domain (residues 102–109) adopts an extended conformation instead of the α-helical conformation seen in the three known cytokine complexes (Figures 1B and 1C). In free IL-17RA, this loop is flanked on either side by the disordered A'A and C'E loops and is stabilized in the crystal by contacts with the D2 domain of a neighboring IL-17RA molecule. Overall, it appears that IL-17 (A, F, or A/F) binding to IL-17RA induces a stable conformation for three flexible, disordered loops of the free D1 domain and that these structural changes are associated with a conformational switch of the BC loop from a random coil to an α-helical structure.

An IL-17RA dimer is present in all crystal structures of IL-17RA binary complexes

The BC loop mentioned above and the three disordered loops in the unliganded IL-17RA structure are involved in conspicuous crystal contacts that are consistently found—but have been overlooked thus far—in the binary complexes of IL-17RA with IL-17A, IL-17F, and IL-17A/F, despite different crystallization conditions, unit cell dimensions, and crystal symmetries (Ely et al., 2009; Liu et al., 2013; Goepfert et al., 2017) (Figure 2). These crystal contacts form an IL-17RA homodimerization interface of about 750–820 Å^2 that is only absent in the crystal structure of the free IL-17RA receptor reported here. We used the EPPIC protein-protein interface classifier (Duarte et al., 2012) to investigate its potential biological relevance. This method analyzes evolutionary pressure on interface residues using closely related homologs to distinguish mere crystal lattice contacts from biologically relevant interfaces. When applied to the three available IL-17RA binary complexes, EPPIC consistently classified the IL-17RA - IL-17RA dimer interface as biologically relevant and identified residues Thr69, Thr102, Asp103, Ala104, and Ser105 as core interface residues with very low sequence entropy, based on a sequence alignment with 78 close homologs (sequence identity >60%) (Tables S3 and S4 and Figure S1). This prediction, combined with our structural observation that the A'A, C'E, FG, and BC loops did not have the conformation required for homodimerization in the unliganded IL-17RA receptor, raised the possibility that the structural changes of the D1 domain upon IL-17 (A, F, or A/F) binding and the subsequent dimerization of IL-17RA might be a prelude to the assembly of the signaling complex.

Author Manuscript Author Manuscript Author Manuscript Author Manuscript

IL-17-induced IL-17RA dimerization controls the architecture of the heteromeric signaling complex

Through extensive crystallization screening and optimization, we obtained crystals of the ternary complex of human IL-17A with the extracellular domains of its two cognate receptors, IL-17RA and IL-17RC (Tables S1 and S2). While these crystals only diffracted to a maximum resolution of 5.1 Å, structure determination by molecular replacement, using the X-ray structures of IL-17RC (PDB: 6hg4) and of the IL-17A-IL-17RA complex (PDB: 4hsa), was straightforward. Because of the limited resolution, the structure did not provide reliable atomic details of individual amino acid side-chains, but it did reveal the overall composition and quaternary structure of the IL-17A signaling complex (Figure 3). The asymmetric unit of the crystal contained one IL-17A homodimer flanked by one IL-17RA and one IL-17RC subunit, in an arrangement that confirmed the validity of a recently published, tentative model of the heterotrimeric complex (Goepfert et al., 2020). A superimposition with the binary IL-17RA - IL-17A complex did not reveal any significant domain shifts (Figure S2). However, inspection of the crystal packing revealed a structural feature that had not been anticipated, the dimerization of the heterotrimeric complex driven by the same IL-17RA-IL-17RA interface as seen in all IL-17RA binary complexes (Figures 2 and 3B). The full signaling complex may thus comprise two heterotrimeric units related by a crystallographic 2-fold symmetry axis to form a 2:2:2 hexameric complex (2 × IL-17RA, 2 × IL-17RC, 2 × IL-17A homodimers) (Figure 3B). No higher order oligomerization state was found by visual inspection and EPPIC analysis of the crystal packing.

The dimerization of the heterotrimeric complex did not create any additional subunit-subunit interface within the signaling assembly except between the two IL-17RA D1 domains: each IL-17A homodimer interacted with only one IL-17RA and one IL-17RC subunit, and the two co-receptors were not in contact with each other. IL-17RC was located at a distance from the IL-17RA dimerization interface and did not contribute to dimerization (Figure 3B). However, the formation of this hexameric assembly defines the relative position of the two IL-17RC stalks (Goepfert et al., 2020) and is therefore likely to play an important role in assembling the intracellular signaling machinery.

As expected from the known crystal structures of IL-17RA-IL-17A (Liu et al., 2013) and IL-17RC-IL-17F (Goepfert et al., 2020), the amino-terminal FnIII domains (D1) of IL-17RA and IL-17RC interacted with equivalent binding pockets located on either side of the cytokine homodimer (Figure 3A). The following FnIII domain (D2) adopted a different orientation in the two receptors but formed otherwise similar interactions with the cytokine, notably a β-sheet/ β-strand interaction with the C-terminal residues of IL-17A, as previously observed in IL-17A and IL-17F binary complexes (Figure S3). Like in the IL-17RC-IL-17F complex (Goepfert et al., 2020), the D3–D4 domains of IL-17RC did not contribute any contacts to the cytokine and appeared to act as a sturdy stalk, whereas IL-17RA was connected to the cell membrane via a flexible 17-amino acid linker, not defined in this structure (Figure 3A). This loose connection between the IL-17RA ECD and its intracellular domains suggested that IL-17RC may play a key structural role in driving the spatial organization of the intracellular signaling components, while IL-17RA dimerization plays a more indirect, yet no less important structural role in defining the precise geometry of

Author Manuscript Author Manuscript Author Manuscript Author Manuscript

the two IL-17RC subunits and ensuring that their juxtamembrane regions are about 90 Å apart in the hexameric complex. These structural inferences further suggested that IL-17RA dimerization may have functional implications for IL-17 signaling.

IL-17A binding induces IL-17RA dimerization in solution

We therefore set out to investigate whether IL-17RA dimerization induced by IL-17A binding could also be observed in solution and used site-directed mutagenesis for generating a dimerization-defective IL-17RA variant. We looked for a critical residue near the center of the dimerization interface and selected alanine 104 on the basis of the EPPIC analysis combined with visual inspection of the IL-17RA dimer interface on a 3D display. Ala104 is located within the α-helical region of the BC loop, at the heart of the IL-17RA-IL-17RA protein-protein interface. This residue was identified as a core interface residue with very low sequence entropy by the EPPIC web server (Table S4 and Figure S1). It is exposed on the surface of the IL-17RA monomer, but its solvent-accessible surface is reduced by 99% upon receptor dimerization. The two alanine 104 residues in the IL-17RA dimer are 7 Å apart. We reasoned that the replacement of alanine 104 by a glutamate (A104E point mutant) would prevent dimerization through steric hindrance and repulsive electrostatic interactions (Figures 3B and S4). Each of the two Glu104 side-chains would collide with Leu68, Thr70, Pro71, Ser105, and Tyr108 of the opposite IL-17RA subunit and would be located in a mainly hydrophobic environment. Binding of IL-17A to IL-17RA, however, should not be affected by this mutation, because it is located at a distance (21 Å) from the cytokine-binding region, and it is facing bulk solvent in the absence of dimerization; also, like alanine, glutamate has a high helix-forming propensity, and it is therefore not likely to interfere with the IL-17RA motions induced by IL-17A binding, including the conformational switch of the BC loop.

We first analyzed the binding of IL-17A to wild-type (WT) and A104E IL-17RA by surface plasmon resonance (SPR) and isothermal titration calorimetry (ITC).

SPR analyses confirmed that the A104E point mutation had no significant effect on the affinity and binding kinetics of IL-17A to IL-17RA (Figure 4A). The K_D value for the WT IL-17RA complex with IL-17A (5.2 nM) was well in agreement with a previous determination using the same technology (2.8 nM; Ely et al., 2009). Using ITC, we observed very similar isothermal titration profiles, indicating that the A104E point mutation did not affect the thermodynamics and binding stoichiometry of the cytokine to the IL-17RA receptor (Figure 4B). The stoichiometry inferred from the ITC data was consistent with one IL-17A homodimer binding only one IL-17RA receptor subunit, in line with crystallographic findings (Liu et al., 2013). Note that dimerization of IL-17RA does not change the overall stoichiometry of the IL-17A-IL-17RA complex. The similar ITC profiles indicated that the much smaller IL-17RA dimerization interface (~750–820 $Å^2$ compared with ~2022–2070 $Å^2$ for the IL-17A/IL-17RA binding interface) contributed little, if at all, to the overall enthalpy. Alternatively, or in addition, only a fraction of all IL-17A complexes with the IL-17RA ECD may have formed 2:2 complexes under these experimental conditions. It is unclear why the K_D values obtained by ITC were significantly weaker than those determined by SPR. Previous ITC analyses of IL-17RA and IL-17RC

Author Manuscript Author Manuscript Author Manuscript Author Manuscript

binary complexes have also suggested weaker affinities (Goepfert et al., 2020) compared with SPR measurements (Ely et al., 2009).

Next, we investigated the influence of the A104E point mutation on the formation of the binary complex with IL-17A and of the ternary complex with IL-17A and IL-17RC by analytical size-exclusion chromatography coupled to a multi-angle light scattering apparatus (SEC-MALS). This experiment showed clear differences between the WT IL-17RA and the A104E point mutant (Figure 5). Whereas the mutant IL-17RA receptor formed a 1:1 binary complex with the expected molecular weight (MW) of about 61 kDa, the WT receptor had a much shorter elution time and was nearly two times bigger (115 kDa), indicating a 2:2 complex (2 × IL-17RA, 2 X IL-17A homodimers). In presence of IL-17RC, the A104E mutant formed the expected heteromeric 1:1:1 complex with IL-17A (observed MW of 131 kDa). WT IL-17RA exhibited a significantly higher MW of about 165 kDa. This observation confirmed a previous SEC-MALS analysis of the heterotrimeric complex (Goepfert et al., 2020). At the time, we were not aware of IL-17A-induced IL-17RA dimerization and concluded that the 1:1:1 complex was in equilibrium with a higher order oligomer that was an integer multiple of the 1:1:1 complex, as shown by high-performance liquid chromatography (HPLC) quantification of the protein components. In the light of the crystallographic data, consistently showing dimerization of IL-17RA complexes, we can now interpret the observed molecular weight of 165 kDa as being a weighted average indicative of an equilibrium between the 2:2:2 heteromeric complex (calculated MW 258 kDa) and the 1:1:1 complex (calculated MW 129 kDa), under these experimental conditions. Importantly, while the A104E mutation did not affect binding of IL-17A to IL-17RA, as shown by SPR and ITC, it clearly suppressed the formation of higher MW complexes in the SEC-MALS experiment, further supporting our conclusion that IL-17A-induced IL-17RA dimerization was also taking place in solution and was responsible for the increase in the apparent MW of the heteromeric complex. While dimerization of the IL-17RA ECD was not complete in the SEC-MALS experiment, it is conceivable that the full-length transmembrane IL-17RA receptor may form stronger dimeric complexes within the plane of the cell membrane, with its intracellular domains potentially also contributing to dimerization.

IL-17RA dimerization lowers the threshold for IL-17A and IL-17F signaling

In order to investigate potential functional consequences of IL-17RA dimerization, we then generated an IL-17RA knockout N/TERT keratinocyte cell line (Dickson et al., 2000) and retrovirally introduced either WT IL-17RA or the A104E point mutant cDNAs under control of the EF1α promoter. In order to avoid clonal differences, we used stable WT or A104E IL-17RA cell pools for our analysis. These stable cell pools were confirmed to display similar levels of human IL-17RA protein on the cell surface (Figure S5) and exhibited similar *IL36G* and *CXCL1* mRNA induction following TNFα stimulation (Figure S6).

In agreement with our biophysical data (Figure 4), the mutation did not affect cytokine recognition: biotinylated IL-17A displayed a very similar level of binding to A104E and WT IL-17RA cells by flow cytometry (EC_{50} values of 586 ng/mL and 486 ng/mL, respectively) (Figure 6). Likewise, binding of biotinylated IL-17F to A104E and WT IL-17RA cells was in a similar range (EC_{50} values 184 μg/mL and 393 μg/mL, respectively) (Figure 6).

Author Manuscript Author Manuscript Author Manuscript Author Manuscript

In contrast to experiments using TNFα stimulation (Figure S6), A104E IL-17RA cells showed a clear reduction in responsiveness compared with the WT IL-17RA cells when IL-17A or IL-17F stimulation was used, irrespective of the presence or absence of a fixed concentration of 1 ng/mL TNFα (Figures 7A and 7B). Whereas WT IL-17RA cells required 0.36 ± 0.11 ng/mL or 1.14 ± 0.67 ng/mL IL-17A (with and without TNFα, respectively) for half-maximal response (EC_{50}) in *IL36G* mRNA induction, A104E cells required >5-fold more IL-17A in order to achieve half-maximal response (EC_{50} values of 1.91 ± 0.59 ng/mL and 6.64 ± 1.64 ng/mL with and without TNFα, respectively) (Figure 7A). A similar shift in responsiveness was also seen for IL-17F, where WT IL-17RA cells required 10.0 ± 2.0 ng/mL (with TNFα) or 41.9 ± 10.4 ng/mL (without TNFα) IL-17F for half-maximal response (EC_{50}) in *IL36G* mRNA induction, while A104E cells required >6-fold higher IL-17F concentrations for half-maximal response (EC_{50} values of 64.7 ± 26.7 ng/mL and 264 ± 96 ng/mL when stimulated with or without TNFα, respectively) (Figure 7B). A reduced responsiveness to IL-17 cytokines of the A104E IL-17RA cells compared with the WT IL-17RA cells was also observed for *CXCL1* gene induction (Figure 7C).

DISCUSSION

Human IL-17A was originally identified from a library of $CD4^+$ T cells (Yao et al., 1995). The subsequent discovery of the Th17 cell lineage and its implication in numerous chronic inflammatory and autoimmune diseases has drawn much attention to the role of IL-17A in the adaptive immune response. However, IL-17A and IL-17F are also produced by many cell types of the innate immune system and play important roles in the early inflammatory immune response (Veldhoen, 2017; McGeachy et al., 2019). IL-17A and IL-17F synergize with several cytokines of the innate immune response, including IL-1β, IL-18, IL-22, and TNFα, in inducing a strong inflammatory response mediated by IL-6 production. The IL-17 signaling pathway shares important nodes with other receptors of the innate immune response, such as the TNF receptor family, the TLRs, and the interleukin-1 (IL-1) receptors (IL-1Rs), notably TRAF6, TAK1, IKKγ, nuclear factor-κB, AP-1, c-Jun N-terminal kinase, and p38 MAPK (Amatya et al., 2017; Li et al., 2019).

Full-length, membrane-bound IL-17RA has been reported to self-associate in the absence of ligand (Kramer et al., 2006, 2007), and forced over-expression of both IL-17RA and IL-17RC was not sufficient for ligand-independent signal transduction (Toy et al., 2006). These findings have led to the hypothesis that unliganded IL-17RA remains in an inactive state through homotypic interactions, and that ligand binding triggers rapid conformational changes that relieve these interactions and foster productive, heterotypic interactions with IL-17RC (Toy et al., 2006). Whether these homotypic interactions involve the extracellular (ECD) or the intracellular domains or both is not known. Our work focused on the recombinant, soluble IL-17RA ECD. The analysis of the crystal packing of the IL-17RA ECD in the ligand-free state did not reveal any crystal contacts that would be suggestive of homotypic interactions, indicating that homotypic IL-17RA interactions may rather involve the intracellular domains. In contrast, the comparison of the free and cytokine-bound states of the IL-17RA ECD revealed cytokine-induced structural changes that affect four loops of the D1 domain, and an elbow movement of the D2 domain that leads to a significant shift (11–17 Å, depending on the IL-17 cytokine) of the juxta-membrane region and

Author Manuscript Author Manuscript Author Manuscript Author Manuscript

may therefore play a role in relieving intracellular homotypic interactions. Moreover, the structural changes of the D1 domain enable dimerization of the IL-17RA-cytokine complex through the formation of a sizable IL-17RA-IL-17RA interface that involves the upper part of this domain. While the size of this interface falls in the range (600–1200 $Å^2$) where differentiating biologically irrelevant crystal lattice contacts from biologically relevant interfaces can be difficult, EPPIC analysis, which considers the conservation through evolution of interface residues, indicated a potential biological significance. The pervasive occurrence of this IL-17RA dimer interface in three different IL-17RA-cytokine complexes, and across distinct crystal forms and crystallization conditions, further supported a potential biological significance. Lastly, the observation that IL-17RA receptor dimerization appeared to require cytokine binding strongly spoke in favor of a potential regulatory mechanism, which deserved further investigations, including biochemical, biophysical, and cell-based experiments using a dimerization-defective point mutant of human IL-17RA.

Our biochemical and biophysical analyses confirmed that the designed A104E mutation in the IL-17RA ECD did not affect IL-17A binding. Evidence for dimerization of the WT IL-17RA binary and ternary complexes but not of the corresponding A104E IL-17RA complexes was obtained by SEC-MALS analysis. Under the SEC-MALS experimental conditions, dimerization was not complete, suggesting rather weak IL-17RA dimers when the receptor is truncated to its ECD and analyzed in solution. Conceivably, the full transmembrane IL-17RA receptor may form stronger dimers because of its reclusion within the membrane and through additional interactions with intracellular components of the signaling machinery. While the A104E point mutation did hamper dimerization of the binary and ternary complexes of the soluble IL-17RA ECD in the SEC-MALS experiment, we cannot rule out the possibility that, in our cellular experiments, the correct assembly of the intracellular signaling machinery is only compromised but not fully blocked by this mutation. Hence, our cellular data might not reveal the functional importance of IL-17RA dimerization to its full extent. Nevertheless, these data clearly indicate that the dimerization of the heteromeric receptor complex into a hexameric signalosome has a functional importance: it lowers the IL-17A and IL-17F signaling threshold for *IL36G* and *CXCL1* mRNA induction in human N/TERT keratinocytes, presumably through more efficient recruitment of downstream effectors such as the membrane proximal effectors ACT1 and TRAF6. Further investigations are clearly needed to gain a broader overview of the functional consequences of IL-17-induced dimerization of IL-17RA for other IL-17 family members that also use IL-17RA as co-receptor and for other cell types such as fibroblasts.

The picture that is emerging from this work, however, is a mechanism whereby IL-17RA receptor sharing by IL-17 family members is not only governed by the intrinsic flexibility of these cytokines (Waters et al., 2021) but also by order/disorder transitions of ligand-binding loops within the D1 domain of the receptor and by the fine adjustment of the position of its D2 domain. Starting from the resting state of the IL-17RA receptor, the rotation of the D2 domain and the subsequent receptor homodimerization induced by IL-17 binding are a likely prelude to the assembly of the membrane-proximal signaling machinery. This molecular mechanism, seen with IL-17A, IL-17F, and IL-17A/F, may also hold for IL-17C and IL-17E, which also use IL-17RA as co-receptor.

Author Manuscript Author Manuscript Author Manuscript Author Manuscript

IL-17RA is a “short” receptor, characterized by a flexible, 17-amino-acid-long segment connecting its cytokine-binding domains to the cell membrane (Goepfert et al., 2020). In the case of IL-17A, IL-17F, and IL-17A/F, IL-17RA associates with IL-17RC to form the heteromeric 2:2:2 signaling complex. In contrast to IL-17RA, IL-17RC is a “tall” receptor that possesses a rigid stalk connecting its cytokine-binding domains to the cell membrane (Goepfert et al., 2020). Therefore, the two IL-17RC subunits within the hexameric signalosome, in the configuration imposed by the geometry of the IL-17RA dimer, appear to play a key role in driving the proper spatial organization of the intracellular signaling machinery through their rigid stalk and transmembrane region. As IL-17RE is also a tall receptor, IL-17C signaling probably follows a similar molecular mechanism. The situation is less clear for IL-17E, which signals through two short receptors, IL-17RA and IL-17RB, and for IL-17A when it uses IL-17RD, another short receptor, in combination with IL-17RA.

While this report describes IL-17-induced IL-17RA dimerization and its role in assembling the IL-17 signaling complex, much of the corresponding biology remains to be explored. Our preliminary data suggest that blocking IL-17RA dimerization, eventually with a therapeutic agent, will only reduce and not abrogate downstream IL-17RA-dependent IL-17 signaling. Whether such a strategy would lead to a distinct, beneficial clinical outcome in some indications, or eliminate potential side effects compared with fully antagonistic anti-IL-17RA therapeutics, is unclear at present.

Limitations of the study

Our biophysical experiments were performed with the soluble, extracellular domains of IL-17RA and IL-17RC; therefore, our data may not faithfully reflect the oligomerization behavior of the full-length receptors in the cell membrane. In particular, it is unclear whether IL-17-induced IL-17RA dimerization leads to increased avidity of (potentially oligomeric) full-length IL-17RC for the IL-17RA/IL-17A complex. While our cellular experiments clearly show reduced IL-17A and IL-17F signaling in immortalized human keratinocytes overexpressing the dimerization-defective IL-17RA A104E variant, the impact of this mutation on the full IL-17 signaling complex (extracellular and intracellular) at natural expression levels and in primary human cell lines is not known. Consequently, further investigations are needed to gain a deeper understanding of the functional importance of IL-17RA dimerization *in vivo* and to unravel how IL-17RA dimerization potentiates IL-17 signaling at the molecular level.

STAR★METHODS

RESOURCE AVAILABILITY

Lead contact—Further information and requests for resources and reagents should be directed to and will be fulfilled by the Lead Contact, Jean-Michel Rondeau (jeanmichel.rondeau@novartis.com).

Materials availability—Requests regarding the N/TERT cell lines should be directed to Johann E. Gudjonsson (johanng@med.umich.edu). All other unique reagents generated

Author Manuscript Author Manuscript Author Manuscript Author Manuscript

in this study are available from the lead contact with a completed Materials Transfer Agreement.

Data and code availability

- Crystallographic atomic coordinates and structure factors have been deposited in the Protein Data Bank (www.rcsb.org) with accession codes 7zan: IL-17A/IL-17RA/IL-17RC complex; 5n9b: unliganded IL-17RA.
- This paper does not report original code.
- Any additional information required to reanalyze the data reported in this paper is available from the lead contact upon request.

METHOD DETAILS

Cloning—For cellular studies, full-length IL-17A (amino acid residues 1–155 of Uniprot:Q16552) with the native signal peptide and full-length IL-17F (amino acid residues 31–163 of Uniprot:Q96PD4) fused to the Myeloid cell surface antigen CD33 signal peptide (UniProt: P20138–1) were cloned into a pCI-derived co-expression vector. To facilitate purification, a synthetic peptide with the amino acid sequence EFRHDS derived from the human Amyloid Precursor protein (APP6-tag) was fused N-terminally to the IL-17F chain (Goepfert et al., 2017).

For ITC, SEC-MALS and crystallisation, a DNA construct of IL-17A (34–155) lacking the first 10 residues of the mature IL-17A and with the N68D and C129S point mutations, as used by Liu and colleagues (Liu et al., 2013) was cloned into a pCI-derived vector. The DNA sequence was fused with an N-terminal Myeloid cell surface antigen CD33 signal peptide (UniProt: P20138–1) followed by the EFRHDS peptide and a PreScission recognition sequence (LEVLFQGP). Several IL-17RA constructs were tried in crystallisation trials. The full-length extracellular domain (ECD) of IL-17RA (amino acid residues 33–320 of UniProt: Q96F46) fused to the CD33 protein signal peptide and a C-terminal APP6-Avi-tag was cloned in a pRS5-derived vector. This construct enabled the X-ray analysis of IL-17RA in the unliganded state. For the crystallisation of the ternary complex, a more convenient IL-17RA construct with a shorter APP-tag (amino acids sequence: EFRH; “APP4-tag”) and three N-linked glycosylation sites removed by replacing Asn with Asp at positions 49, 206 and 265 gave the best diffracting crystals. Site-directed mutagenesis was performed on the latter construct to generate the A104E point mutant for SPR, ITC and SEC-MALS studies. The full-length ECD domain of IL-17RC (amino acid residues 21–467 of UniProt:Q8NAC3-2, Q307R variantHaudenschild et al., 2002) fused to the CD33 protein signal peptide and a C-terminal APP6-tag was cloned in a pRS5-derived vector.

Protein expression and purification—IL-17A/F, IL-17A, IL-17RA, A104E IL-17RA, and IL-17RC were transiently expressed in human embryonic kidney (HEK) 293–6E cells or, alternatively, in GnTI-deficient HEK293S cells (RRID:CVCL_A785) for the purpose of crystallisation trials.

Author Manuscript Author Manuscript Author Manuscript Author Manuscript

Transient co-expression of IL-17A and IL-17F in HEK 293S cells led to the production of IL-17A, IL-17F and of the IL-17A/F heterodimer. The three isoforms (IL-17A, IL-17F and IL-17A/F) were separated by affinity chromatography using NHS-activated resin coupled to an anti-APP-tag antibody. While the IL-17A homodimer was in the flow-through, the IL-17A/F heterodimer and the IL-17F homodimer were retained on the column and eluted with 0.1 M glycine, pH 2.7. pH was immediately restored by addition of 1.0 M of Tris, pH 8.5. IL-17A was further purified by affinity chromatography with the human anti-IL-17A monoclonal antibody XAB4 (WO 2014/122613 A1) and eluted as before. IL-17A/F was separated from IL-17F homodimers using the same affinity chromatography. The isolated IL-17A, IL-17A/F and IL-17F proteins were further purified by size exclusion chromatography (SEC) with a Superdex-75 10/300 (GE Healthcare) in PBS pH 7.4, 1mM EDTA.

All IL-17RA ECD constructs were also purified by anti-APP affinity chromatography, followed by SEC on a Superdex-200 26/600 (GE Healthcare).

For IL-17RC, an additional purification step was used. After affinity purification, the protein was applied to a Resource-Q anion exchange column (Amersham Biosciences) and eluted with a linear gradient of NaCl. Pooled fractions were further purified by SEC as before.

APP-tagged IL-17A was also purified by affinity capture as before. The APP-tag was then cleaved with PreScission protease overnight at 4°C. Tag-free protein was further purified by SEC using a Superdex-75 10/300 in PBS pH 7.4, 1mM EDTA.

Untagged IL-17A constructs used in SPR and SEC-MALS were expressed in *E. coli* BL21(DE3)T1 cells as inclusion bodies. For IL-17A(31–155), cells were lysed with a French press in 50mM Tris pH 8.0, 5mM EDTA, 5mM DTT, 5mM benzamidine. After centrifugation, inclusion bodies were washed 3 times in lysis buffer, followed by three washing steps using 50mM Tris pH 8.0, 300mM NaCl, 1.0% Triton and two more washing steps with 10mM DTT. Inclusion bodies were then dissolved in 6.0M guanidine, 20mM Tris pH 8.5, 100mM NaCl, 10mM DTT. After centrifugation, the supernatant was diluted at room temperature under stirring in refolding buffer containing 20mM Tris pH 9.0, 500mM Arginine-HCl, 15% glycerol, 1mM cystamine, 5mM L-cysteine, and then stirred further at 4°C for two days. After filtration, concentration, and dialysis against 20mM MES pH 6.0, 20mM NaCl, the refolded material was loaded onto an XK 26/10 SP-Sepharose HP column (GE Healthcare) and eluted with a 0.02–1.0M NaCl gradient. Fractions containing covalent IL-17A homodimers were identified by non-reducing SDS-PAGE, pooled, and further purified by reverse phase chromatography on an XK26/10 Source 30 RPC column (Cytiva), using a 0–90% acetonitrile, 0.1% TFA gradient, followed by chromatography over an MPC ceramic hydroxyfluoro-apatite column (Bio-Rad Laboratories), and by cation-exchange chromatography on a Mono-S HR 1010 column (GE Healthcare). After each chromatographic steps, fractions containing covalent IL-17A homodimers were identified by non-reducing SDS-PAGE, pooled and analyzed by LC-MS.

For the IL-17A(34–155)_C129S construct which lacks the inter-chain disulfide bridges, a simplified refolding and purification protocol was used. The cell pellet was resuspended

Author Manuscript Author Manuscript Author Manuscript Author Manuscript

in lysis buffer (50mM Tris pH 8.0, 300mM NaCl, 1mM $MgCl_2$, 100μg/mL lysozyme, 200μg/mL DNaseI, 1 tablet of protease inhibitor cocktail) and lysed with a French press. After centrifugation, inclusion bodies were washed 2 times in 2M urea, 5mM DTT, 2% Triton X-100, 50mM Tris pH 8.0, followed by two more washing steps using 100mM Tris pH 8.0. Inclusion bodies were then solubilised in 6.0M guanidine, 50mM Tris pH 8.0, 50mM NaCl. After centrifugation, the supernatant was diluted 20-fold dropwise, at room temperature under stirring, into a refolding buffer containing 50mM Tris pH 8.5, 500mM guanidine, 0.4M arginine, 2mM reduced glutathione, 1mM oxidised glutathione, and then stirred further at 4°C overnight. The refolding mix was then centrifuged, filtered and concentrated. After overnight dialysis against 50mM MES pH 6.0, centrifugation and filtration, the refolded material was purified on a Mono-S column (GE Healthcare) followed by size-exclusion chromatography with a Superdex75 column in 25mM HEPES, pH 7.5, 150mM NaCl.

Crystals of IL-17RA in the free state were obtained using the wild-type IL-17RA(33–320)-APP_6-Avi construct. To facilitate crystallization, the APP-Avi-tag was removed by treatment with Carboxypeptidase A (Sigma-Aldrich, MO, USA) for 3 days at room temperature and the reaction stopped by adding 1mM EDTA. The protein was further treated with Endoglycosidase H (Sigma-Aldrich, MO, USA) for 4h at 37°C and purified by size-exclusion chromatography in 10 mM Tris (pH 7.5), 100 mM NaCl. The protein was concentrated to 8.7 mg Ml^{-1}.

The IL-17RA/IL-17A/IL-17RC complex was formed by mixing the Endoglycosidase H-treated receptors IL-17RC(21–467)-APP6 and IL-17RA(33–320)_N49D_N206D_N265D-APP_4 and the cytokine IL-17A(34–155)_N68D_C129S with a 1.2-fold molar excess of receptors. The complex was purified by size-exclusion chromatography with a Superdex-200 16/600 equilibrated with PBS pH 7.4, 10 mM EDTA and concentrated to 7.5 mg mL^{-1}.

Biotinylation—To enable cell binding measurements, chemical biotinylation of IL-17A and IL-17F was performed with a 5- and 10-fold excess, respectively, of EZ-Link-Sulfo-NHS-LC-LC-Biotin (cat.no. 21338; Thermo Fisher Scientific) in PBS pH 7.4. After one hour incubation at room temperature, the reaction was stopped with 1M Tris pH 8.0 and the excess biotin removed by running the sample on a SPX75 10/30 equilibrated with PBS pH 7.4.

Crystallization—Initial crystals were obtained at 20°C using the sitting-drop vapor diffusion method after mixing 0.2 μL protein solution with 0.2 μL reservoir solution. Unliganded IL-17RA crystallized from 0.1 M Tris-HCl (pH 7.0), 25% (w/v) PEG MME 2000, 0.05 M lithium sulfate monohydrate. Crystals of the IL-17A complex with IL-17RA and IL-17RC were initially obtained from 14% v/v PEG MME 500, 0.1M MES pH 6.5. These crystals were optimized using the microseeding technique. Seeds were prepared by crushing crystals with the “seed-bead” kit from Hampton Research and were resuspended in the mother liquor. Microseeding was carried out by mixing 1 μL protein solution with 0.8 μL reservoir solution containing 10% v/v PEG DME 500, 0.1M MES pH 6.5 and 0.2 μL seeding solution. Crystals of the complex were transferred for 2 min in a cryo-protecting buffer composed of 0.1M HEPES pH 7.0, 5% PEG 4,000, 25% glycerol, whereas no

Author Manuscript Author Manuscript Author Manuscript Author Manuscript

cryo-protection was needed for the IL-17RA crystals. All crystals were flash-frozen into liquid nitrogen.

Structure determination and refinement—Diffraction data were collected at 100 K at beamline X10SA (PXII) of the Swiss Light Source (λ = 1.0000Å) with a PILATUS pixel detector. In total, 720 images of 0.25° oscillation each were recorded at a crystal-to-detector distance of 300mm and 720mm for the free IL-17RA receptor and the ternary complex, respectively. The IL-17RA data were processed with XDS version September 26, 2012 and were scaled and merged with XSCALE version July 4, 2012 (Kabsch, 1993; RRID: SCR_015652). The IL-17A ternary complex was processed with autoPROC 1.1.7 (20210716) (Vonrhein et al., 2011; RRID:SCR_015748), using a resolution cut-off based on the $CC^{1/2}$ statistics (Karplus and Diederichs, 2012, 2015). The use of the $CC^{1/2}$ statistics led to a resolution cut-off of 5.06Å, compared to 6.15Å when using a more conservative cut-off based on mean $I/\sigma(I) > 2.0$. STARANISO analysis showed some anisotropy with diffraction limits of 6.07Å along c* and 5.09Å for the other two ellipsoid axes. No evidence was found for pseudo-translation, twinning, higher symmetry, or pseudo-symmetry.

Both structures were determined by maximum likelihood molecular replacement with PHASER (McCoy et al., 2007; RRID:SCR_014219). For the free IL-17RA structure, the two FnIII domains of IL-17RA (chain C of PDB: 4hsa (Liu et al., 2013), residues 2–172 and 173–273, respectively) were used as independent search models. Several rounds of iterative model building and refinement were performed with Coot 0.8.6 (Emsley et al., 2010; RRID:SCR_014222) and autoBUSTER version 2.11.6 (Bricogne et al., 2021; RRID:SCR_015653), respectively.

The structure of the ternary complex of IL-17A with IL-17RA and IL-17RC was determined with PHASER 2.8.3 using the binary complex with IL-17RA (chains ABC of PDB: 4hsa), and the D1 and D2D3D4 domains of IL-17RC from PDB: 6hg4 as search models. After an initial rigid-body refinement of all protein domains with autoBUSTER, the structure was further refined with autoBUSTER and PHENIX_ROSETTA (DiMaio et al., 2013; Liebschner et al., 2019; RRID: SCR_014224), using secondary-structure restraints and reference-model (Headd et al., 2012) or target-structure (Smart et al., 2012) restraints based on PDB:6hg4 (IL-17RC D1, 3.32Å), PDB: 6hga (IL-17RC D2D3D4, 2.6Å), PDB: 5n9b (IL-17RA, 1.9Å) and an *in house*, high resolution (1.27Å) structure of human IL-17A. Only one translation/libration/screw (TLS) group was refined per protein chain (Afonine et al., 2018). The inclusion of all hydrogen atoms with null occupancy was essential for maintaining good geometry. A subset of 5% of the diffraction data were excluded from refinement and used for cross-validation (Brünger, 1992). Refinement protocols which led to a lower Rfree at the expense of increased overfitting (as judged by a larger difference between Rfree and Rwork) were discarded. The final model was produced by autoBUSTER. The autoBUSTER electron-density maps revealed N-glycosylation of Asn54 of IL-17RA and of Asn213, Asn226 and Asn349 of IL-17RC. The highest positive peak of the F(early)-F(late) Fourier map was located at the position of the IL-17RA Cys43 disulfide-bridge. Among the remaining 18 peaks greater than 3 standard deviations above the mean, another four were located on disulfide bridges (Cys146B of IL-17A; Cys338 of IL-17RC, Cys196 of IL-17RA, Cys144B of IL-17A), two others on aspartic acid (Asp29 and Asp45 of

Author Manuscript Author Manuscript Author Manuscript Author Manuscript

IL-17RC) and two more on glutamic acid side-chains (Glu141 of IL-17RC, Glu136A of IL-17A). The geometry of the final model was assessed using the PHENIX implementation of Molprobity (Williams et al., 2018). Buried solvent-accessible surfaces of protein-protein interfaces were computed with the program AREAIMOL from the CCP4 program suite using default parameters (Winn et al., 2011; RRID:SCR_007255). All figures were prepared with PyMol version 2.5.2 (Schrödinger LLC; RRID:SCR_000305).

ITC—ITC was performed with a MicroCal Auto-ITC_{200} calorimeter (Malvern Instruments, UK) at 298K. Proteins were dialyzed overnight against the same reaction buffer (PBS pH 7.4, 1mM EDTA). Protein concentration was quantified by monitoring UV absorbance at 210nm using High-Performance Liquid Chromatography (HPLC). All titrations were made by 26 successive 3s injections of 1.5μL cytokines into 120μL of IL-17RA solution with a 180s interval between consecutive injections. An initial delay of 60s was applied before the first injection and a stirring speed of 750rpm was applied. For the wild-type receptor, the experiment was performed with 250μM IL-17A (syringe) and 35μM IL-17RA (cell). For the experiment with the A104E receptor variant, 149μM IL-17A and 22μM A104E IL-17RA were used. The binding isotherms were fitted to a single-site binding model under the MicroCal PEAQ-ITC analysis software (version 1.21, Malvern Instruments, UK).

SPR—The binding affinity of IL-17A toward wt IL-17RA and the A104E variant was determined by surface plasmon resonance measurements using a MASS2 instrument (Sierrasensors). Protein concentrations were quantified by monitoring UV absorbance at 210nm using High-Performance Liquid Chromatography (HPLC). IL-17A was diluted at 5μg/mL in 10mM HEPES pH 7.5 and immobilized by direct coupling on SPR Affinity Sensors, High Capacity Amine (Sierrasensors) to a level of approximately 1800RU, using the standard amine coupling procedure (activation with EDC/NHS and deactivation with ethanolamine). For the measurements, IL-17 receptors were diluted in running buffer (PBS pH 7.4, with 3 mM EDTA and 0.05% Tween 20), to a starting concentration of about 20–50 times the K_D, and serial dilutions in two-fold increments were made (highest concentrations were 100nM for wt IL-17RA and 250nM for the A104E variant). To determine kinetic constants, sensorgrams were collected at 22°C with a flow rate of 25μL/min. Each protein was loaded for 200s with a dissociation time of 300s. The sensor chip surface was regenerated between runs with 3.0M $MgCl_2$. All experiments were performed four times independently. All data were analyzed with the MASS2 evaluation software and fitted to a 1:1 Langmuir binding model.

SEC-MALS—SEC-MALS experiments were performed at room temperature with an analytical Superdex 200 3.2/300 Increase SEC column, using an Äkta micro system (GE Healthcare) coupled to a miniDAWN TREOS triple-angle light-scattering detector equipped with an Optilab T-rEX refractive index detector (Wyatt Technology). The column was pre-equilibrated with running buffer (20mM Na-phosphate pH 7.4, 150mM NaCl, 0.02% sodium azide). 25–100μg of protein were diluted into 60μL of running buffer and 50μL were run on the SEC column at a flowrate of 0.075mL/min. For the IL-17A binary complex with IL-17RA, a 1.2-fold molar excess of cytokine was used. For the IL-17A ternary complex with IL-17RC and IL-17RA, the cytokine was mixed with a 1.1-fold molar excess of

Author Manuscript Author Manuscript Author Manuscript Author Manuscript

IL-17RC followed by addition of 1.1-fold molar excess of IL-17RA. UV, light scattering and refractive index values were recorded. Peaks of interest were manually selected, and data analysis was carried out with the ASTRA software (version 5.3, Wyatt Technology; RRID:SCR_016255).

Generation of IL-17RA KO keratinocytes by CRISPR/cas9—Human immortalized keratinocyte N/TERT cells (Dickson et al., 2000; RRID:CVCL_CW92) were cultured in keratinocytes-SFM medium (Gibco #17005042) supplemented with 30μg/mL bovine pituitary extract (BPE), 0.2ng/mL EGF and 0.3mM Ca^{2+} final concentration.

CRISPR KO keratinocytes were generated by an insertion or deletion of a single or multiple nucleotides induced by a single guide RNA (sgRNA) designed from the 5′ end of the coding sequence/ORF of the target gene. sgRNA target sequence (TCCCCGTGGCTCACATCGAA) for IL-17RA was generated using a web interface for CRISPR design (https://portals.broadinstitute.org/gpp/public/analysis-tools/sgrna-design). Two synthetic oligos, IL17RAsgRNA-F: CACCGTCCCCGTGGCTCACATCGAA and IL17RAsg RNA-R: AAACTTCGATGTGAGCCACGGGGAC (IL-17RA sgRNA target sequence and its complementary sequence flanked by adapter sequences corresponding to the BBS-I cut site) were purchased from Millipore-Sigma. These two oligos were annealed and then ligated into a CRISPR backbone vector, pSpCas9 (BB)-2A-GFP (PX458; a gift from Feng Zhang (Addgene plasmid # 48138)) by T4 ligase. Ligated plasmids were cloned into competent *E. coli* (ThermoFisher # C737303) and sgRNA target sequence insertion was verified by Sanger sequencing. The plasmid was transfected into an immortalized keratinocyte line (N/TERT) using the TransfeX transfection kit (ATCC # ACS4005). GFP positive single cell sorting was performed into 96-well plate using a MoFlo Astrios #1 cell sorter at the University of Michigan Flow Cytometry Core. Single cell colonies were grown up to ~50% confluency. Cells were then transferred from 96-well plates into 12-well plates and grown again up to ~50% confluence. Each clone was then divided into two parts, with one part used to isolate DNA for genotyping and the other part stored for further analysis after completing genotyping. DNA was extracted and PCR was performed using two primers (IL17RAPCRF1: GATTCACCCTCGAAACCTGA and IL17RAPCRR1: CTGACTGGGAGAGCCACTTG) spanning the sgRNA target sequence of IL-17RA. We confirmed homozygous mutant clone with 14 nucleotides deletion. For validation of findings, a total of three independent CRISPR/Cas9 KO mutants were generated for IL-17RA.

Generation of stable cell pools—Complementary DNAs (cDNAs) encoding the full-length human wild type IL-17RA (wtIL-17RA, transcript variant 1, NCBI NM_014339.7) or the human A104E IL-17RA mutant were cloned into the lentiviral expression vector (pCDH-EF1α-MCS-T2A-hygro) containing the EF1α promotor and a hygromycin B selection cassette resulting in the two vectors, pCDH-EF1-IL17RA-WT and pCDH-EF1-IL17RAmut. For the generation of pCDH-EF1α-MCS-T2A-hygro, the puromycin selection cassette of pCDH-EF1α-MCS-T2A-puro (System Biosciences LLC, CD527A-1) was replaced with a hygromycin B selection cassette. For the generation of wt IL-17RA and A104E IL-17RA N/TERT cells using lentiviral transduction, 1.5×10^6 293T cells were

Author Manuscript Author Manuscript Author Manuscript Author Manuscript

seeded into 6-well plates. The next morning, cells were transfected with 1μg of above-described lentiviral vectors (pCDH-EF1-IL17RA-WT or pCDH-EF1-IL17-RAmut) together with 1μg of lentiviral packaging plasmid mix (CELLECTA, CPCP-K2A) using TransIT-Lenti Transfection Reagent (Mirus, MIR6600). 48h later supernatants were filtered through a 0.45μm filter (Millipore SLHV013SL) to obtain cell free viral supernatant. N/TERT IL-17RAko cells (passage 6) were seeded into 6-well cell culture plates at 6×10^4 cells/well. Two days after plating, cells were transduced with 1mL of viral supernatant lentivirus for 8 h in the presence of 2μg/mL Polybrene (Sigma #TR1003). 36 h after transduction cells were washed and replated. Stable wt IL-17RA and A104E IL-17RA cell pools were generated by antibiotic selection using 20μg/mL hygromycin B (Invitrogen # 10687010). Transgene expression was verified in each pool by flow cytometry staining for the human IL-17RA receptor (Figure S3).

Flow cytometry analysis

Expression of wild-type and A104E mutant IL-17RA: Adherent N/TERT keratinocyte cells were dissociated using Accutase (Promocell cat#41310) to obtain a single cell suspension. For the detection of cell surface expression of IL-17RA receptor on IL-17RAko, wt IL-17RA and A104E IL-17RA cells, cells were stained with Alexa Fluor® 488-conjugated anti-IL-17RA antibody (R&D Systems cat# FAB177G) or isotype control antibody Alexa Fluor488-conjugated msIgG1 (IC002F, R&D Systems) for 30 min on ice. Cells were washed once before flow cytometry analysis using a Fortessa LSR flow cytometer (BD Biosciences).

Binding of IL-17A and IL-17F to IL-17RA KO, wt IL-17RA and A104E IL-17RA N/TERT cells: Cells were incubated with serial dilutions of biotinylated IL-17A or IL-17F and cell surface bound cytokines were detected by flow cytometry using Alexa Fluor™ 647 conjugated Streptavidin, (Thermofisher #S32357). Analysis and visualization of flow cytometry data was done using FlowJo version 10.7.1 (RRID:SCR_008520).

Functional assay—Wild-type IL-17RA and A104E IL-17RA N/TERT hygromycin B selected cell pools were cultured at 37°C, 5% CO_2 in keratinocyte-SFM medium (Gibco #17005042) supplemented with 30μg/mL bovine pituitary extract (BPE), 0.2ng/mL EGF, 20μg/mL hygromycin B and 0.3mM Ca^{2+} final concentration. IL-17A and IL-17F stimulation of cells was done in presence or absence of a fixed concentration of 1ng/mL TNFα (Novartis #BTP14065) for 6 h. After stimulation, cells were lysed using RLT lysis buffer (Qiagen cat# 79216) containing 40mM dithiothreitol (DTT, Sigma cat#: 3483–12-3) and total RNA was isolated using the RNeasy Mini kit (Qiagen cat#: 74106). One-step qRT-PCR was done according to the manufacturers' instructions (TaqMan® RNA-to-Ct™ 1-Step Kit Thermofisher # 4392656) using primer probe sets (Thermofisher) for human *IL36G* (Hs00219742_m1) and *CXCL1* (Hs00236937_m1). Quantification of gene expression was performed using the $\Delta\Delta C_T$ method (Livak and Schmittgen, 2001) and normalized to the housekeeping gene *RPLPO* (Hs99999902_m1).

Author Manuscript Author Manuscript Author Manuscript Author Manuscript

QUANTIFICATION AND STATISTICAL ANALYSIS

Data were analyzed using GraphPad PRISM 9.12 (RRID:SCR_002798). For each experiment, replicates were performed as indicated in the figure and table legends and all results are shown as the mean value ± SEM. Statistical significance of each group was determined using the unpaired Student's t test (Student's t test for unpaired samples).

Supplementary Material

Refer to Web version on PubMed Central for supplementary material.

ACKNOWLEDGMENTS

We thank Felix Freuler and Simon Haenni for the cloning of IL-17RC, IL-17RA, and IL-17A constructs, Sandra Kapps-Fouthier for support with protein expression, and Patrick Graff for LC-MS analyses of recombinant proteins. We thank eXpose and the SLS PXII beamline staff for expert X-ray data collection. We are grateful to Pr. Dr. Timm Maier (Biozentrum, Basel) for stimulating discussions and advice. This work was supported by a Presidential Postdoc Fellowship awarded to A.G. by the Novartis Institutes for BioMedical Research (NIBR) Postdoc Office. J.E.G. and M.K.S. are supported by NIH P30 AR075043 and the Taubman Medical Research Institute. N.L.W. was supported by NIH P50 AR070590 and NIH R01 AR062546.

REFERENCES

Adams PD, Afonine PV, Bunkóczi G, Chen VB, Davis IW, Echols N, Headd JJ, Hung L-W, Kapral GJ, Grosse-Kunstleve RW, et al. (2010). PHENIX: a comprehensive python-based system for macromolecular structure solution. Acta Crystallogr. D Biol. Crystallogr. 66, 213–221. 10.1107/S0907444909052925. [PubMed: 20124702]

Afonine PV, Adams PD, and Urzhumtsev A (2018). From deep TLS validation to ensembles of atomic models built from elemental motions. II. Analysis of TLS refinement results by explicit interpretation. Acta Crystallogr. D Struct. Biol. 74, 621–631. 10.1107/S2059798318005764. [PubMed: 29968672]

Amatya N, Garg AV, and Gaffen SL (2017). IL-17 signaling: the yin and the yang. Trends Immunol. 38, 310–322. 10.1016/j.it.2017.01.006. [PubMed: 28254169]

Beringer A, Noack M, and Miossec P (2016). IL-17 in chronic inflammation: from discovery to targeting. Trends Mol. Med. 22, 230–241. 10.1016/j.molmed.2016.01.001. [PubMed: 26837266]

Bricogne G, Blanc E, Brandl M, Flensburg C, Keller P, Paciorek W, Roversi P, Sharff A, Smart OS, Vonrhein C, and Womack TO (2021). BUSTER Version 2.11.8 (Global Phasing Ltd).

Brünger AT (1992). Free R value: a novel statistical quantity for assessing the accuracy of crystal structures. Nature 355, 472–475. 10.1038/355472a0. [PubMed: 18481394]

Chang SH, Park H, and Dong C (2006). Act1 adaptor protein is an immediate and essential signaling component of interleukin-17 receptor. J. Biol. Chem. 281, 35603–35607. 10.1074/jbc.C600256200. [PubMed: 17035243]

Chung S-H, Ye X-Q, and Iwakura Y (2021). Interleukin-17 family members in health and disease. Int. Immunol. 33, 723–729. 10.1093/intimm/dxab075. [PubMed: 34611705]

Cua DJ, and Tato CM (2010). Innate IL-17-producing cells: the sentinels of the immune system. Nat. Rev. Immunol. 10, 479–489. 10.1038/nri2800. [PubMed: 20559326]

Deng C, Peng N, Tang Y, Yu N, Wang C, Cai X, Zhang L, Hu D, Ciccia F, and Lu L (2021). Roles of IL-25 in Type 2 inflammation and autoimmune pathogenesis. Front. Immunol. 12, 691559. 10.3389/fimmu.2021.691559. [PubMed: 34122457]

Dickson MA, Hahn WC, Ino Y, Ronfard V, Wu JY, Weinberg RA, Louis DN, Li FP, and Rheinwald JG (2000). Human keratinocytes that express hTERT and also bypass a p16INK4a-enforced mechanism that limits life span become immortal yet retain normal growth and differentiation characteristics. Mol. Cell Biol. 20, 1436–1447. 10.1128/MCB.20.4.1436-1447.2000. [PubMed: 10648628]

Author Manuscript Author Manuscript Author Manuscript Author Manuscript

DiMaio F, Echols N, Headd JJ, Terwilliger TC, Adams PD, and Baker D (2013). Improved low-resolution crystallographic refinement with Phenix and Rosetta. Nat. Methods 10, 1102–1104. 10.1038/nmeth.2648. [PubMed: 24076763]

Draberova H, Janusova S, Knizkova D, Semberova T, Pribikova M, Ujevic A, Harant K, Knapkova S, Hrdinka M, Fanfani V, et al. (2020). Systematic analysis of the IL-17 receptor signalosome reveals a robust regulatory feedback loop. EMBO J. 39, e104202. 10.15252/embj.2019104202. [PubMed: 32696476]

Duarte JM, Srebniak A, Schärer MA, and Capitani G (2012). Protein interface classification by evolutionary analysis. BMC Bioinformatics 13, 334. 10.1186/1471-2105-13-334. [PubMed: 23259833]

Ely LK, Fischer S, and Garcia KC (2009). Structural basis of receptor sharing by interleukin 17 cytokines. Nat. Immunol. 10, 1245–1251. 10.1038/ni.1813. [PubMed: 19838198]

Emsley P, Lohkamp B, Scott WG, and Cowtan K (2010). Features and development of Coot. Acta Crystallogr. D Biol. Crystallogr. 66, 486–501. 10.1107/S0907444910007493. [PubMed: 20383002]

Ferrao R, Li J, Bergamin E, and Wu H (2012). Structural insights into the assembly of large oligomeric signalosomes in the Toll-Like receptor-interleukin-1 receptor superfamily. Sci. Signal. 5, re3. 10.1126/scisignal.2003124. [PubMed: 22649099]

Gaffen SL, Jain R, Garg AV, and Cua DJ (2014). The IL-23-IL-17 immune axis: from mechanisms to therapeutic testing. Nat. Rev. Immunol. 14, 585–600. 10.1038/nri3707. [PubMed: 25145755]

Glassman CR, Mathiharan YK, Jude KM, Su L, Panova O, Lupardus PJ, Spangler JB, Ely LK, Thomas C, Skiniotis G, and Garcia KC (2021). Structural basis for IL-12 and IL-23 receptor sharing reveals a gateway for shaping actions on T versus NK cells. Cell 184, 983–999.e24. 10.1016/j.cell.2021.01.018. [PubMed: 33606986]

Goepfert A, Lehmann S, Wirth E, and Rondeau J-M (2017). The human IL-17A/F heterodimer: a two-faced cytokine with unique receptor recognition properties. Sci. Rep. 7, 8906. 10.1038/s41598-017-08360-9. [PubMed: 28827714]

Goepfert A, Lehmann S, Blank J, Kolbinger F, and Rondeau J-M (2020). Structural analysis reveals that the cytokine IL-17F forms a homodimeric complex with receptor IL-17RC to drive IL-17RA-independent signaling. Immunity 52, 499–512.e5. 10.1016/j.immuni.2020.02.004. [PubMed: 32187518]

Haudenschild D, Moseley T, Rose L, and Reddi AH (2002). Soluble and transmembrane isoforms of novel interleukin-17 receptor-like protein by RNA splicing and expression in prostate cancer. J. Biol. Chem. 277, 4309–4316. 10.1074/jbc.M109372200. [PubMed: 11706037]

Headd JJ, Echols N, Afonine PV, Grosse-Kunstleve RW, Chen VB, Moriarty NW, Richardson DC, Richardson JS, and Adams PD (2012). Use of knowledge-based restraints in phenix.refine to improve macromolecular refinement at low resolution. Acta Crystallogr. D Biol. Crystallogr. 68, 381–390. 10.1107/S0907444911047834. [PubMed: 22505258]

Kabsch W (1993). Automatic processing of rotation diffraction data from crystals of initially unknown symmetry and cell constants. J. Appl. Crystallogr. 26, 795–800. 10.1107/S0021889893005588.

Karplus PA, and Diederichs K (2012). Linking crystallographic model and data quality. Science 336, 1030–1033. 10.1126/science.1218231. [PubMed: 22628654]

Karplus PA, and Diederichs K (2015). Assessing and maximizing data quality in macromolecular crystallography. Curr. Opin. Struct. Biol. 34, 60–68. 10.1016/j.sbi.2015.07.003. [PubMed: 26209821]

Korn T, Bettelli E, Oukka M, and Kuchroo VK (2009). IL-17 and Th17 cells. Annu. Rev. Immunol. 27, 485–517. 10.1146/annurev.immunol.021908.132710. [PubMed: 19132915]

Kramer JM, Yi L, Shen F, Maitra A, Jiao X, Jin T, and Gaffen SL (2006). Cutting edge: evidence for ligand-independent multimerization of the IL-17 receptor. J. Immunol. 176, 711–715. 10.4049/jimmunol.176.2.711. [PubMed: 16393951]

Kramer JM, Hanel W, Shen F, Isik N, Malone JP, Maitra A, Sigurdson W, Swart D, Tocker J, Jin T, and Gaffen SL (2007). Cutting edge: identification of a pre-ligand assembly domain (PLAD) and ligand binding site in the IL-17 receptor. J. Immunol. 179, 6379–6383. 10.4049/jimmunol.179.10.6379. [PubMed: 17982023]

Author Manuscript Author Manuscript Author Manuscript Author Manuscript

Krstić J, Obradović H, Kukolj T, Mojsilović S, Okić-Dordević I, Bugarski D, and Santibanez JF (2015). An overview of interleukin-17A and interleukin-17 receptor A structure, interaction and signaling. Protein Pept. Lett. 22, 570–578. 10.2174/0929866522666150520145554. [PubMed: 25990083]

Li X, Bechara R, Zhao J, McGeachy MJ, and Gaffen SL (2019). IL-17 receptor–based signaling and implications for disease. Nat. Immunol. 20, 1594–1602. 10.1038/s41590-019-0514-y. [PubMed: 31745337]

Liebschner D, Afonine PV, Baker ML, Bunkóczi G, Chen VB, Croll TI, Hintze B, Hung LW, Jain S, McCoy AJ, et al. (2019). Macromolecular structure determination using X-rays, neutrons and electrons: recent developments in Phenix. Acta Crystallogr. D Struct. Biol. 75, 861–877. 10.1107/S2059798319011471. [PubMed: 31588918]

Liu S, Song X, Chrunyk BA, Shanker S, Hoth LR, Marr ES, and Griffor MC (2013). Crystal structures of interleukin 17A and its complex with IL-17 receptor A. Nat. Commun. 4, 1888. 10.1038/ncomms2880. [PubMed: 23695682]

Livak KJ, and Schmittgen TD (2001). Analysis of relative gene expression data using real-time quantitative PCR and the 2(-Delta Delta C(T)) Method. Methods 25, 402–408. 10.1006/meth.2001.1262. [PubMed: 11846609]

Majumder S, and McGeachy MJ (2021). IL-17 in the pathogenesis of disease: good intentions gone awry. Annu. Rev. Immunol. 39, 537–556. 10.1146/annurev-immunol-101819-092536. [PubMed: 33577346]

McCoy AJ, Grosse-Kunstleve RW, Adams PD, Winn MD, Storoni LC, and Read RJ (2007). Phaser crystallographic software. J. Appl. Crystallogr. 40, 658–674. 10.1107/S0021889807021206. [PubMed: 19461840]

McGeachy MJ, Cua DJ, and Gaffen SL (2019). The IL-17 family of cytokines in health and disease. Immunity 50, 892–906. 10.1016/j.immuni.2019.03.021. [PubMed: 30995505]

Novatchkova M, Leibbrandt A, Werzowa J, Neübuser A, and Eisenhaber F (2003). The STIR-domain superfamily in signal transduction, development and immunity. Trends Biochem. Sci. 28, 226–229. 10.1016/S0968-0004(03)00067-7. [PubMed: 12765832]

Patel DD, and Kuchroo VK (2015). Th17 cell pathway in human immunity: lessons from genetics and therapeutic interventions. Immunity 43, 1040–1051. 10.1016/j.immuni.2015.12.003. [PubMed: 26682981]

Qian Y, Liu C, Hartupee J, Altuntas CZ, Gulen MF, Jane-Wit D, Xiao J, Lu Y, Giltiay N, Liu J, et al. (2007). The adaptor Act1 is required for interleukin 17-dependent signaling associated with autoimmune and inflammatory disease. Nat. Immunol. 8, 247–256. 10.1038/ni1439. [PubMed: 17277779]

Skiniotis G, Boulanger MJ, Garcia KC, and Walz T (2005). Signaling conformations of the tall cytokine receptor gp130 when in complex with IL-6 and IL-6 receptor. Nat. Struct. Mol. Biol. 12, 545–551. 10.1038/nsmb941. [PubMed: 15895091]

Smart OS, Womack TO, Flensburg C, Keller P, Paciorek W, Sharff A, Vonrhein C, and Bricogne G (2012). Exploiting structure similarity in refinement: automated NCS and target-structure restraints in BUSTER. Acta Crystallogr. D Biol. Crystallogr. 68, 368–380. 10.1107/S0907444911056058. [PubMed: 22505257]

Toy D, Kugler D, Wolfson M, Vanden Bos T, Gurgel J, Derry J, Tocker J, and Peschon J (2006). Cutting edge: interleukin 17 signals through a heteromeric receptor complex. J. Immunol. 177, 36–39. 10.4049/jimmunol.177.1.36. [PubMed: 16785495]

Veldhoen M (2017). Interleukin 17 is a chief orchestrator of immunity. Nat. Immunol. 18, 612–621. 10.1038/ni.3742. [PubMed: 28518156]

Vonrhein C, Flensburg C, Keller P, Sharff A, Smart O, Paciorek W, Womack T, and Bricogne G (2011). Data processing and analysis with the autoPROC toolbox. Acta Crystallogr. D Biol. Crystallogr. 67, 293–302. 10.1107/S0907444911007773. [PubMed: 21460447]

Wang X, Lupardus P, LaPorte SL, and Garcia KC (2009). Structural biology of shared cytokine receptors. Annu. Rev. Immunol. 27, 29–60. 10.1146/annurev.immunol.24.021605.090616. [PubMed: 18817510]

Author Manuscript Author Manuscript Author Manuscript Author Manuscript

Waters LC, Veverka V, Strong SL, Muskett FW, Dedi N, Lawson ADG, Prosser CE, Taylor RJ, Henry AJ, and Carr MD (2021). Conformational dynamics in interleukin 17A and 17F functional complexes is a key determinant of receptor A affinity and specificity. Cytokine 142, 155476. 10.1016/j.cyto.2021.155476. [PubMed: 33706174]

Williams CJ, Headd JJ, Moriarty NW, Prisant MG, Videau LL, Deis LN, Verma V, Keedy DA, Hintze BJ, Chen VB, et al. (2018). MolProbity: more and better reference data for improved all-atom structure validation. Protein Sci. 27, 293–315. 10.1002/pro.3330. [PubMed: 29067766]

Winn MD, Ballard CC, Cowtan KD, Dodson EJ, Emsley P, Evans PR, Keegan RM, Krissinel EB, Leslie AGW, McCoy A, et al. (2011). Overview of the CCP4 suite and current developments. Acta Crystallogr. D Biol. Crystallogr. 67, 235–242. 10.1107/S0907444910045749. [PubMed: 21460441]

Yao Z, Fanslow WC, Seldin MF, Rousseau A-M, Painter SL, Comeau MR, Cohen JI, and Spriggs MK (1995). Herpesvirus Saimiri encodes a new cytokine, IL-17, which binds to a novel cytokine receptor. Immunity 3, 811–821. 10.1016/1074-7613(95)90070-5. [PubMed: 8777726]

Author Manuscript Author Manuscript Author Manuscript Author Manuscript

Highlights

- IL-17 (A, A/F, or F) induces IL-17RA dimerization
- IL-17RA dimerization orchestrates the formation of the IL-17 signalosome
- The A104E mutation abrogates IL-17-induced IL-17RA dimerization
- IL-17RA dimerization potentiates IL-17A and IL-17F signaling

Author Manuscript Author Manuscript Author Manuscript Author Manuscript

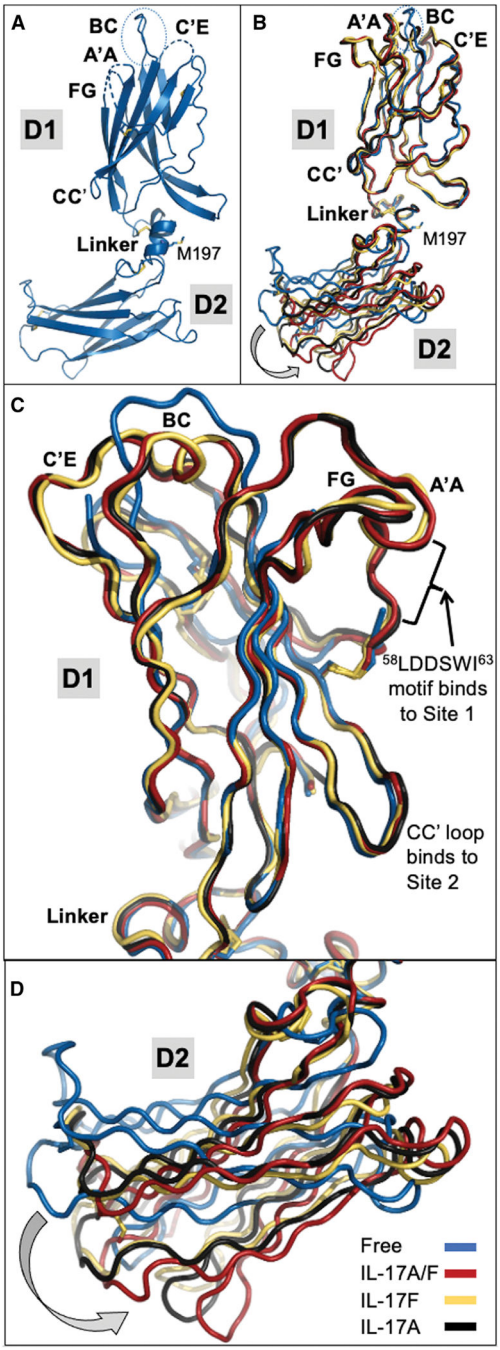

Figure 1. Cytokine binding to IL-17RA induces structural changes in four receptor loops

Structural comparison of unliganded and liganded states of IL-17RA.

(A) Structure of unliganded human IL-17RA, represented as a blue cartoon diagram with the three disordered loops A'A (15 missing residues), C'E (7 missing residues), and FG (9 missing residues) shown as dotted lines and the BC loop highlighted by a dotted ellipsoid.

(B) Structural overlay of the three known liganded states of IL-17RA with IL-17A (black, from PBD: 4hsa), IL-17F (yellow, from PDB: 3jvf), and IL-17A/F (red, from PDB: 5nan) in ribbon representation, with the cytokine ligands omitted for clarity. The overlay is based

Author Manuscript Author Manuscript Author Manuscript Author Manuscript

on the D1 domain only. The orientation is identical to (A). Note the shift of the D2 domain induced by the different IL-17 cytokines, and the structural transition of the BC loop on top (dotted ellipsoid).

(C) Close-up view of the D1 domain, in a different orientation that better shows the conformational switch of the BC loop. Note the key role of the A'A loop in cytokine binding.

(D) Close-up view of the D2 domain. Note the change in the domain orientation in the IL-17A (black), IL-17F (yellow), and IL-17A/F (red) complexes compared with the unliganded state (blue).

Author Manuscript Author Manuscript Author Manuscript Author Manuscript

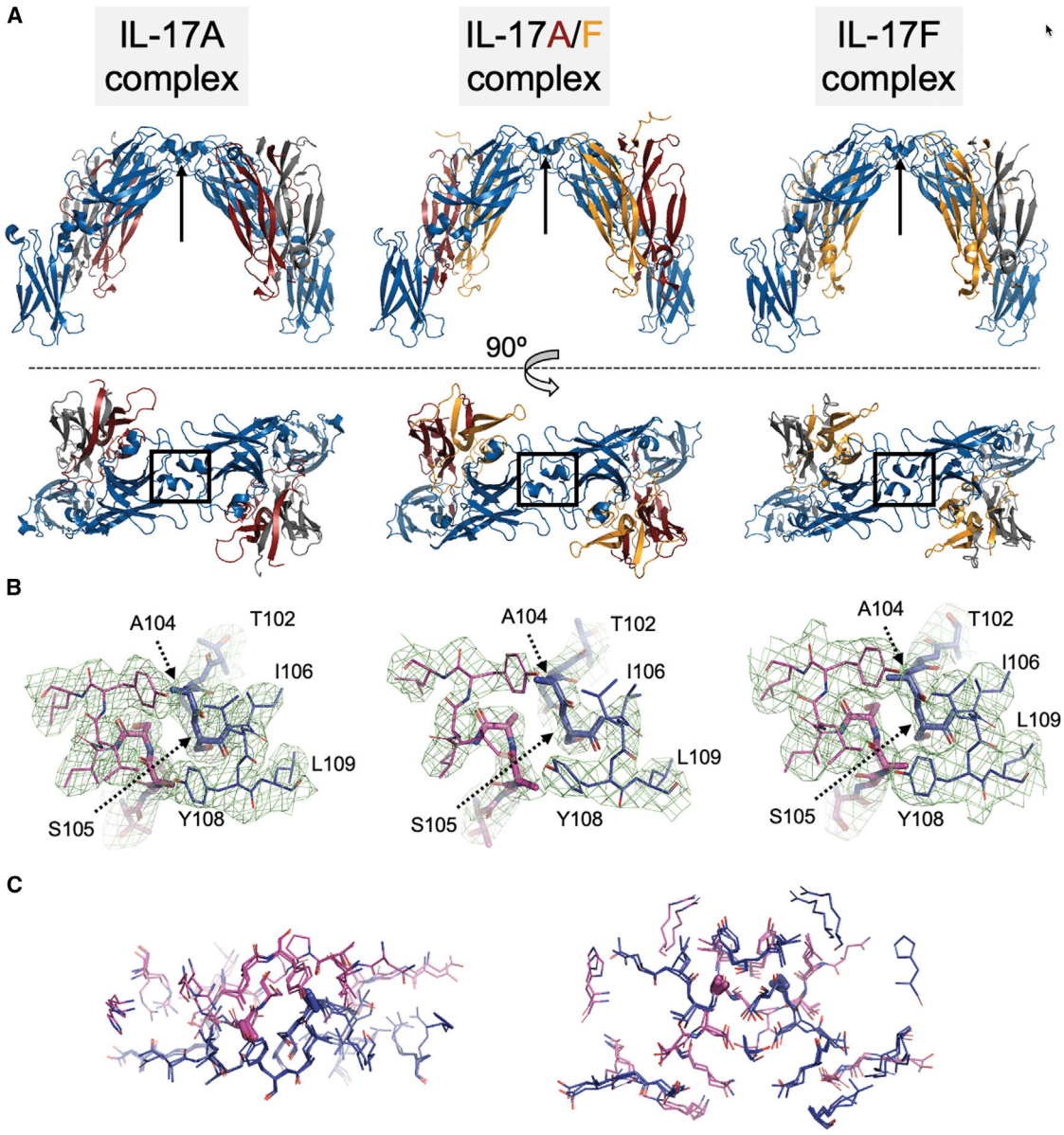

Figure 2. IL-17RA dimers are found in all crystal structures of IL-17RA-IL-17 binary complexes

Conserved crystal contact between two IL-17RA receptor chains (blue ribbon) in the crystal structures of the IL-17A (left view; IL-17A subunits as carmine and gray ribbon, respectively; figure based on PDB: 4hsa), IL-17A/F (center; carmine ribbon: A-subunit; orange ribbon: F-subunit; figure based on PDB: 5nan), and IL-17F complexes (right view; IL-17F subunits as orange and gray ribbon, respectively; figure based on PDB: 3jvf). (A) The top panel shows a side view of two copies of the complex related by exact, crystallographic 2-fold symmetry (IL-17A and IL-17F complexes) or non-crystallographic 2-fold symmetry (IL-17A/F complex). The black arrow points to the BC loop that adopts a helical conformation upon binding of the cytokine and plays a critical role in forming these crystal contacts. The lower panel shows a top view (90° rotation) with the dimerization interface involving the BC loop indicated by a black square. Note that the three

Author Manuscript Author Manuscript Author Manuscript Author Manuscript

X-ray structures were determined from crystals with different unit cells and space group symmetries.

(B) Close-up view of the BC loop at the IL-17RA dimer interface, down the 2-fold symmetry axis. The core interface residues Thr102 to Ser105 (PDB: 5nan numbering scheme) are shown in thick stick representation. The green mesh shows the electron-density map contoured at 1.5σ.

(C) Stereo views showing the full IL-17RA dimer interface from the top (left panel) or from the side (right view). All residues within 4.0 Å from the other subunit are included. The side-chain of Ala104, buried near the center of the interface, is shown in bold stick.

Author Manuscript Author Manuscript Author Manuscript Author Manuscript

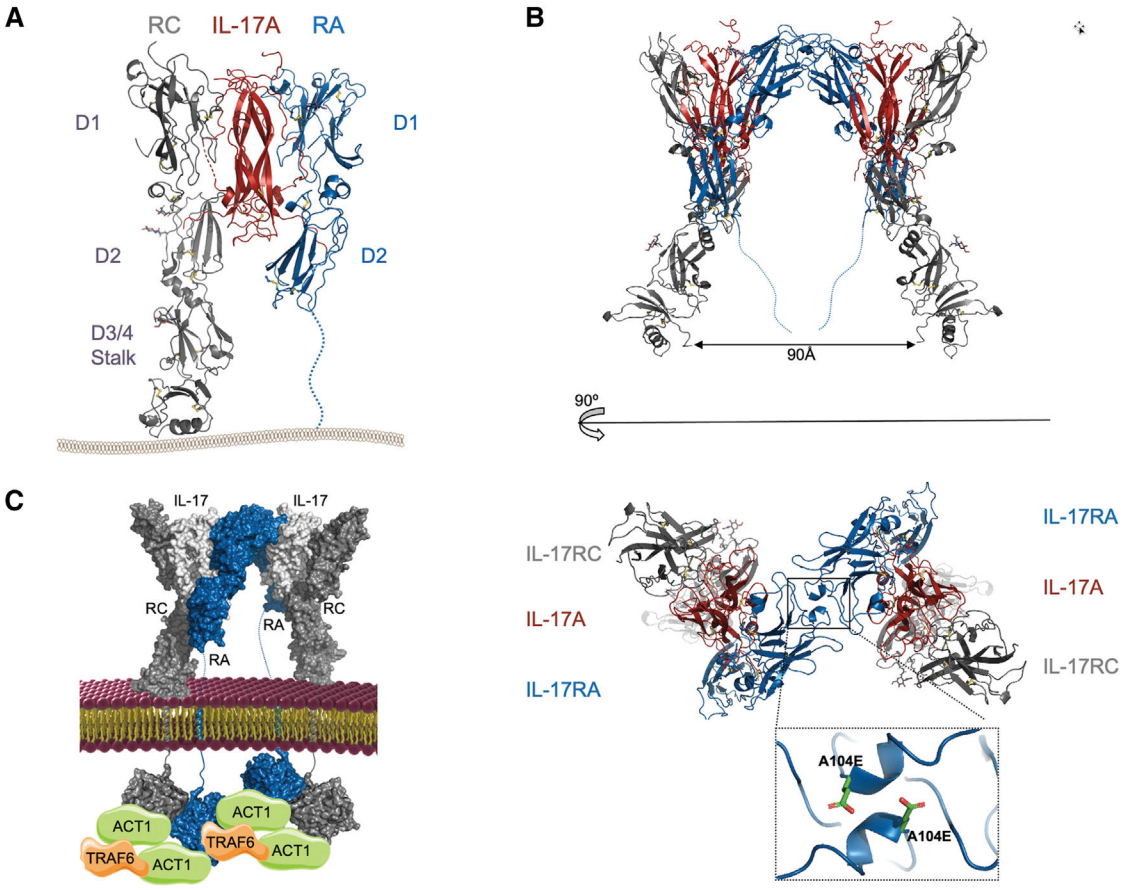

Figure 3. IL-17A-induced dimerization of IL-17RA drives the formation of a 2:2:2 hexameric signalosome

Structure of the heteromeric IL-17A (carmine ribbon) complex with IL-17RA (blue ribbon) and IL-17RC (gray ribbon).

(A) The asymmetric unit contains one-half of the full 2:2:2 complex shown on (B).

(B) Full extracellular, hexameric complex (two views related by 90° rotation). The blue dots represent the flexible linker region of IL-17RA that connects the cytokine-binding domains to the transmembrane region. Note the presence of the same dimerization interface as found in all known IL-17RA binary complexes (Figure 2) and highlighted with a black square. The bottom panel is a close-up view of the IL-17RA dimerization interface. The alanine 104 to glutamate mutation, used in this study to disrupt IL-17RA dimerization, is shown in stick representation.

(C) Schematic model of the IL-17 signalosome; the intracellular SEFIR domains are depicted in arbitrary positions and orientations, with an arbitrary number of Act1 and Traf6 molecules. For more details about the composition of the IL-17 signalosome, please refer to Draberova et al. (2020).

Author Manuscript Author Manuscript Author Manuscript Author Manuscript

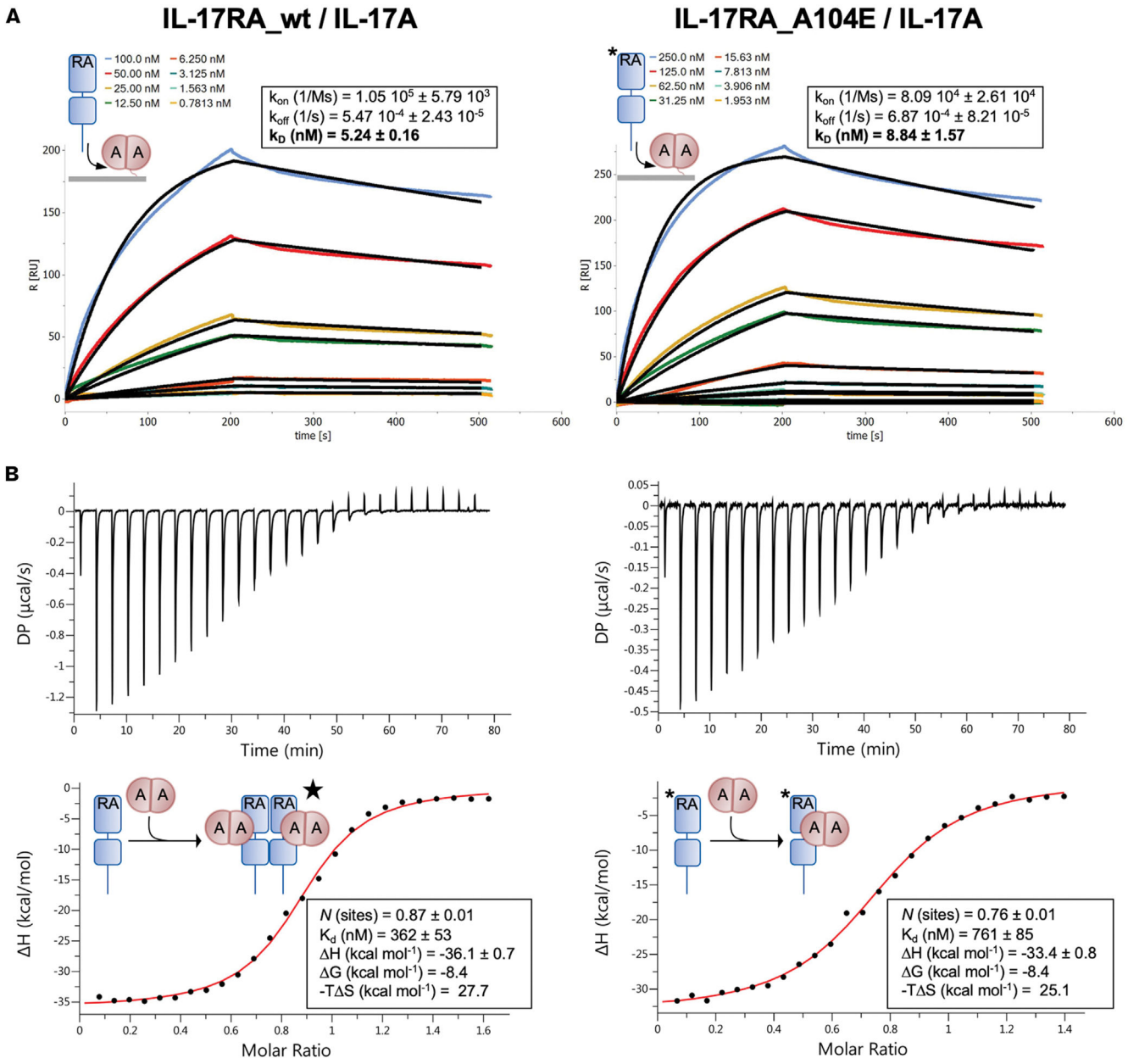

Figure 4. The A104E point mutation does not affect IL-17A binding to IL-17RA

SPR analysis (A) and isothermal calorimetry (B) of IL-17A binding to WT and A104E IL-17RA. (A) Representative sensorgrams are plotted as response in resonance units (RUs) versus time and shown with colored lines. The concentrations of the injected analytes are indicated in the top left corner of the sensorgrams. The kinetic parameters are calculated using a Langmuir 1:1 binding model with the fitted curves depicted as black lines. The indicated Kd represents the mean from four independent experiments ± the standard error of the mean (SEM) and are also summarized in Table S5.

(B) ITC titration curves for the binding of IL-17A to WT and A104E IL-17RA. For each experiment, the top panel shows the raw data with the differential electrical power (DP) plotted against time. The bottom panel represents the binding isotherm (heat change versus

cytokine/receptor molar ratio) obtained from the integration of the raw data and fitted to a “one-site” model. Note that the 2:2 stoichiometry cannot be evidenced from the ITC data; the 2:2 model highlighted with a star sign was inferred from the crystallographic (PDB: 4hsa) and SEC-MALS data.

Author Manuscript Author Manuscript Author Manuscript Author Manuscript

Author Manuscript
Author Manuscript
Author Manuscript
Author Manuscript

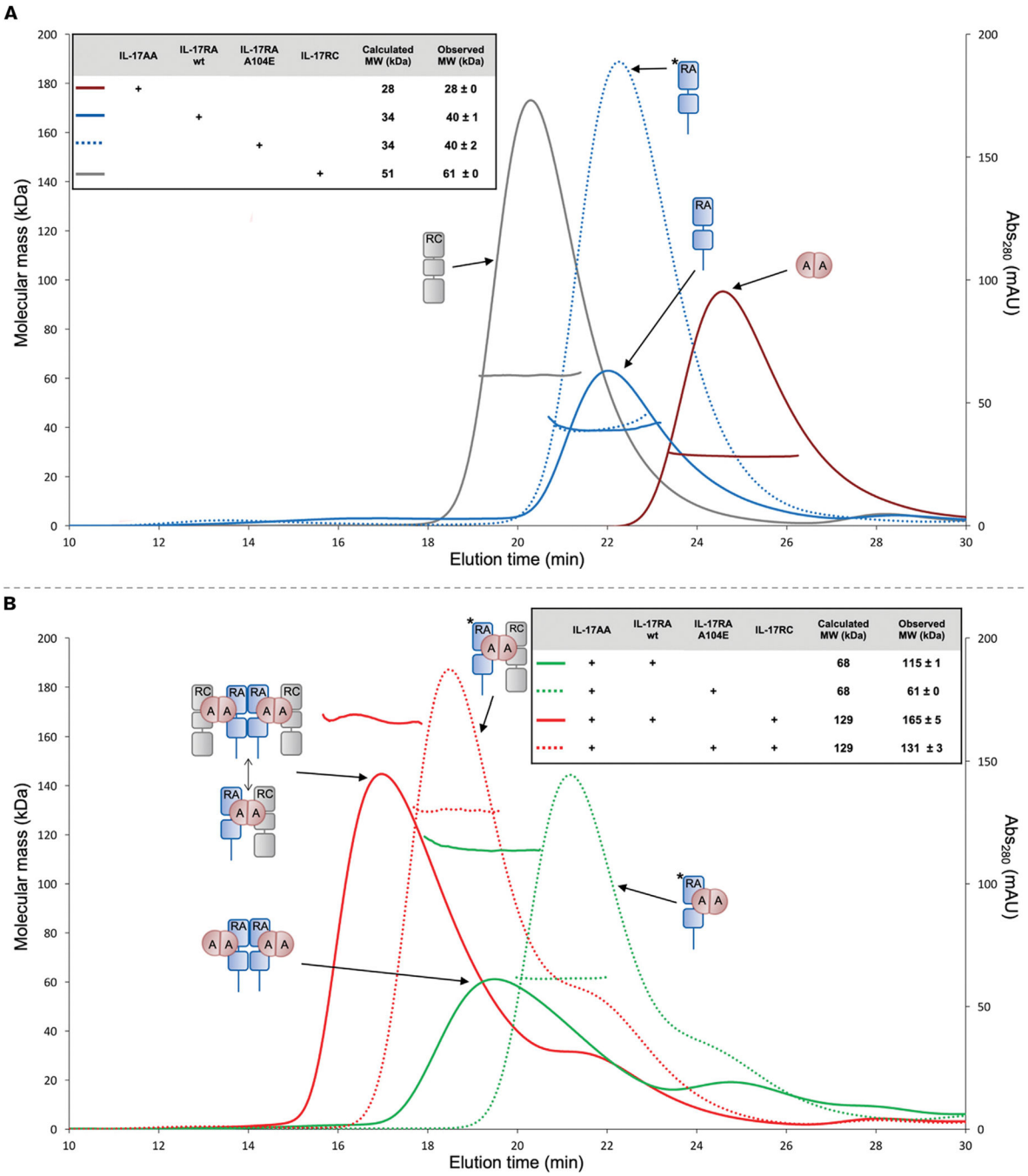

Figure 5. The A104E point mutation blocks IL-17A-induced dimerization of IL-17RA

SEC-MALS analysis of IL-17A binary (IL-17RA) and ternary (IL-17RA/IL-17RC) complexes. SEC chromatograms for isolated proteins (A) and their complexes (B) are color-coded as indicated in the insert table and overlaid with the molecular mass distribution determined by MALS (shown as horizontal lines). Experiments using the A104E IL-17RA point mutant are shown as dotted lines. Peaks are labeled with the corresponding protein or protein complex, depicted schematically, with the star indicating the A104E mutation. The calculated molecular weights in (A) do not consider the glycosylation. Therefore, the

observed values are larger, except for IL-17A, which was expressed in *E. coli* and was thus not glycosylated. For an improved comparison between calculated and observed molecular weights in the case of the receptor complexes, the calculated values in (B) were derived from the observed molecular weights in (A) for the isolated proteins.

Author Manuscript Author Manuscript Author Manuscript Author Manuscript

Author Manuscript Author Manuscript Author Manuscript Author Manuscript

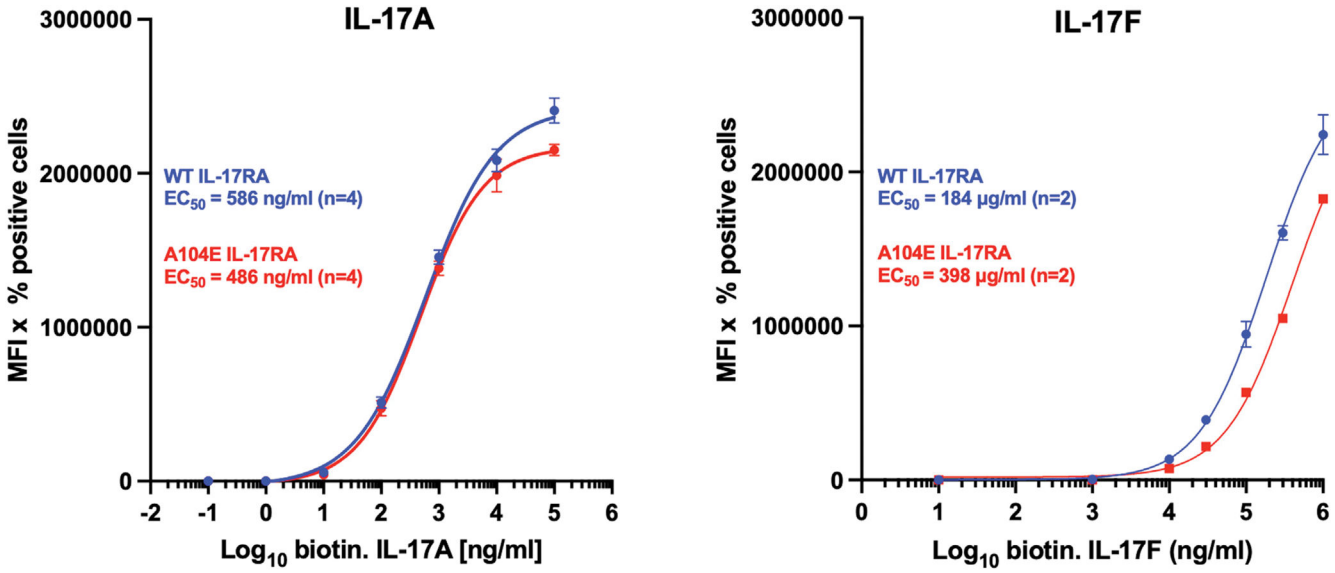

Figure 6. The A104E point mutation does not affect IL-17A or IL-17F binding to N/TERT cells

Binding of IL-17A and IL-17F to WT and A104E IL-17RA cells. Biotinylated human IL-17A (left) or biotinylated human IL-17F (right) was incubated with the cells for 1 h at 4°C, and bound IL-17 was determined by flow cytometry using Alexa Fluor 647 conjugated streptavidin. IL-17A: mean ± standard error of the mean (SEM) (n = 4). IL-17F: mean ± SEM (n = 2); highest possible concentration for IL-17F (1 mg/mL). Color code: blue = IL-17RA WT cells; red = A104E IL-17RA cells.

Author Manuscript Author Manuscript Author Manuscript Author Manuscript

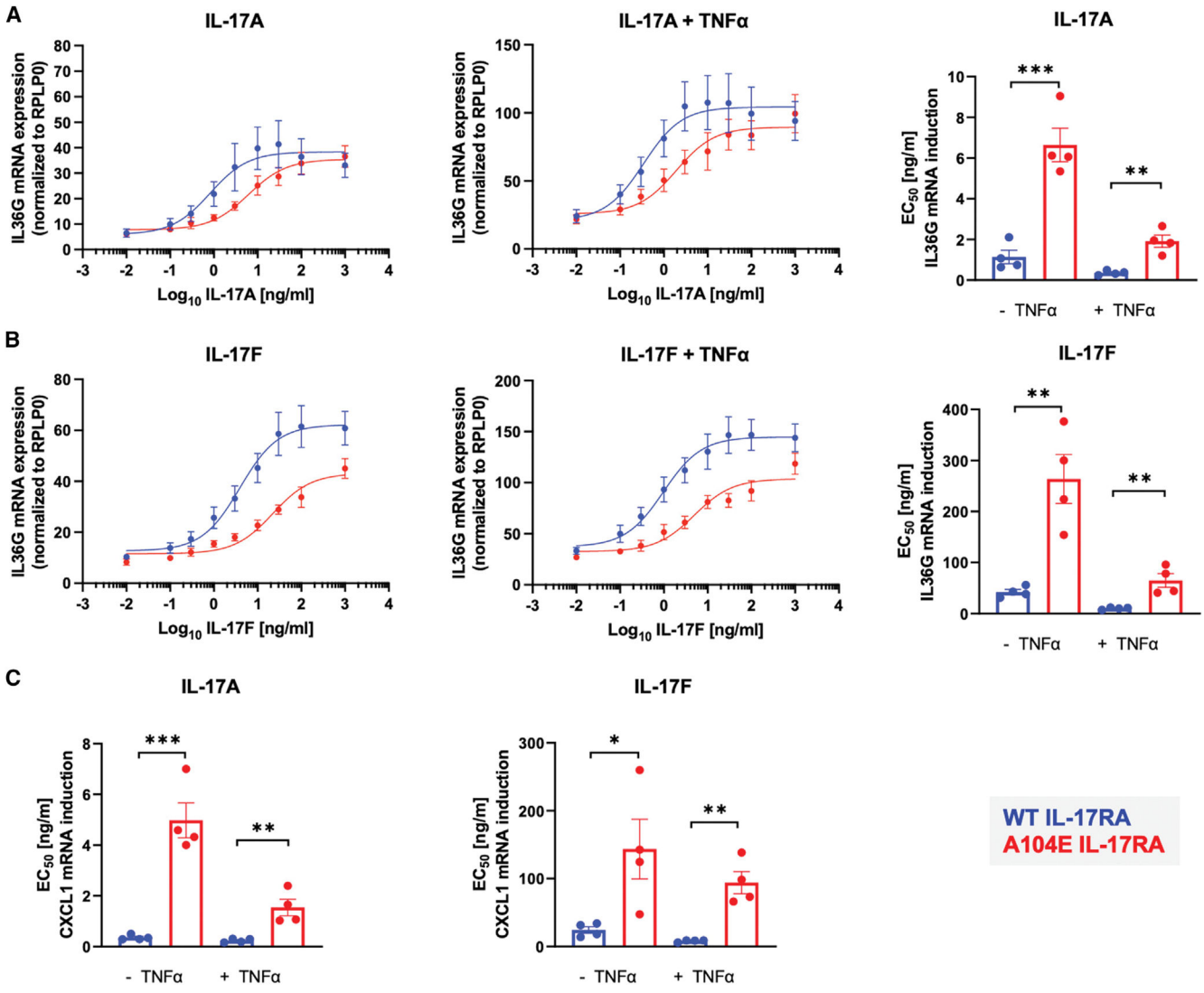

Figure 7. IL-17-induced dimerization of IL-17RA potentiates IL-17 signaling

Functional response of WT and A104E IL-17RA N/TERT cells stimulated for 6 h with (A) IL-17A ± 1 ng/mL TNFα or (B) IL-17F ± TNFα after which *IL36G* mRNA induction was quantified by qRT-PCR. Left side: Concentration-response curves of *IL36G* mRNA induction (n = 4). Right side: EC_{50} values and statistical significance of response between WT and A104E IL-17RA cells. (C) EC_{50} values for *CXCL1* mRNA induction by IL-17A or IL-17F ± 1 ng/mL TNFα in WT and A104E IL-17RA cells. Shown is mean ± SEM (n = 4). *p < 0.05, **p < 0.01, and ***p < 0.001. Color code: blue, WT IL-17RA cells; red, A104E IL-17RA cells.

Author Manuscript Author Manuscript Author Manuscript Author Manuscript

KEY RESOURCES TABLE

REAGENT or RESOURCE	SOURCE	IDENTIFIER
Antibodies		
human anti-human IL-17A antibody XAB4	Novartis	WO 2014/122613 A1
mouse anti-APP tag antibody 6E10-A5	Novartis	N/A
Alexa Fluor® 488-conjugated anti-IL-17RA antibody	R&D Systems	Cat# FAB177G
isotype control Ab Alexa Fluor488- conjugated msIgG1	R&D Systems	Cat # IC002F; RRID:AB_357241
Chemicals, peptides, and recombinant proteins		
hIL-17A, hIL-17F, hIL-17RA, hIL-17RC, hIL-17RA mutants, hTNFα	This paper	N/A
Alexa Fluor™ 647 conjugated Streptavidin	Thermo Fisher Sci.	Cat #S32357
ATCC TransfeX Transfection Reagent	Thermo Fisher Sci.	Cat # ATCC ACS4005
TransIT-Lenti Transfection Reagent	Mirus	Cat # MIR6600
PreScission Protease	GE Healthcare	Cat # 27–0843-01
EndoH	Sigma-Aldrich (Merck)	Cat #11088726001
EZ-link Sulfo NHS-LC-Biotin	Thermo Fisher Sci.	Cat #21338
Deposited data		
IL-17A:IL-17RA:IL-17RC	This paper	PDB: 7ZAN
IL-17RA, unliganded	This paper	PDB: 5N9B
Experimental models: Cell lines		
Human: HEK293-F	Invitrogen	Cat # R79007
Human: HEK293S GnTI-	ATCC	Cat # CRL-3022; RRID:CVCL_A785
Human: immortalized keratinocyte N/TERT cells	Dickson et al. (2000)	RRID:CVCL_CW92
Invitrogen™ One Shot™ Stbl3™ Chemically Competent E. coli	Thermo Fisher Sci.	Cat #C737303
Oligonucleotides		
IL17RAsgRNA-F: CACCGTCCCCGTGGCTCACAT CGAA	Millipore-Sigma	N/A
IL17RAsgRNA-R: AAACTTCGATGTGAGCCACGGGGAC	Millipore-Sigma	N/A
IL17RAPCRF1: GATTCACCCTCGAAACCTGA	Millipore-Sigma	N/A
IL17RAPCRR1: CTGACTG GGAGAGCCACTTG	Millipore-Sigma	N/A
Recombinant DNA		
Plasmid: pSpCas9 (BB)-2A-GFP	Addgene	Addgene_48138
Plasmid: pCDH-EF1 α-MCS-T2A-puro	System Biosciences LLC	Cat # CD527A-1
Plasmid: pCDH-EF1 α-MCS-T2A-hygro	This paper	N/A
Software and algorithms		

Author Manuscript Author Manuscript Author Manuscript Author Manuscript

REAGENT or RESOURCE	SOURCE	IDENTIFIER
Astra, version 5.3	Wyatt	https://www.wyatt.com/products/software/astra.html; RRID:SCR_016255
autoPROC, version 1.1.7	Vonrhein et al. (2011)	https://www.globalphasing.com/autoproc/; RRID:SCR_015748
autoBUSTER 2.11.6	Bricogne et al. (2021)	https://www.globalphasing.com/buster/; RRID:SCR_015653
CCP4, version 7.0.057	Winn etal. (2011)	http://www.ccp4.ac.uk/; RRID:SCR_007255
Coot 0.8.6	Emsley et al. (2010)	http://www2.mrc-lmb.cam.ac.uk/personal/pemsley/coot/; RRID:SCR_014222
FlowJo version 10.7.1.	FlowJo, LLC	https://www.flowjo.com RRID:SCR_008520
GraphPad PRISM 9.12	GraphPad	https://www.graphpad.com/; RRID:SCR_002798
MASS2 evaluation software	Bruker	https://www.bruker.com/
PEAQ-ITC analysis software, version 1.21	Malvern	https://www.malvern.com/en
PHASER 2.6.1	McCoy et al. (2007)	https://www.phenix-online.org/documentation/reference/phaser.html; RRID:SCR_014219
Phenix 1.12	Adams et al. (2010)	https://www.phenix-online.org/; RRID:SCR_014224
Phenix_rosetta	DiMaio et al. (2013)	https://www.phenix-online.org/; RRID:SCR_014224
PyMOL 2.5.2	Schrödinger LLC	http://www.pymol.org/; RRID:SCR_000305
XDS/XSCALE, version Sep. 26, 2012	Kabsch (1993)	http://xds.mpimf-heidelberg.mpg.de/
Other		
keratinocyte-SFM medium	Gibco	Cat # 17005042